

Single-Anchor Localization and Orientation Performance Limits using Massive Arrays: MIMO vs. Beamforming

Anna Guerra, *Member, IEEE*, Francesco Guidi, *Member, IEEE*, Davide Dardari *Senior Member, IEEE*

Abstract—Next generation cellular networks will experience the combination of femtocells, millimeter-wave (mm-wave) communications and massive antenna arrays. Thanks to the beamforming capability as well as the high angular resolution provided by massive arrays, only one single access point (AP) acting as an anchor node could be used for localization estimation, thus avoiding over-sized infrastructures dedicated to positioning. In this context, our paper aims at investigating the localization and orientation performance limits employing massive arrays both at the AP and mobile side. Thus, we first asymptotically demonstrate the tightness of the Cramér-Rao bound (CRB) in massive array regime, and in the presence or not of multipath. Successively, we propose a comparison between MIMO and beamforming in terms of array structure, time synchronization error and multipath components. Among different array configurations, we consider also random weighting as a *trade-off* between the high diversity gain of MIMO and the high directivity guaranteed by phased arrays. By evaluating the CRB for the different array configurations, results show the interplay between diversity and beamforming gain as well as the benefits achievable by varying the number of array elements in terms of localization accuracy.

Index Terms—Position Error Bound, Orientation Error Bound, Millimeter-wave, Massive array, 3D localization, 5G.

I. INTRODUCTION

The widespread use of personal devices generates new challenges while opening new appealing scenarios for future applications, such as, for example, those entailing device-to-device (D2D) interactions or Big Data management issues. To meet these new trends, different disruptive technologies have been recently proposed for the next fifth generation (5G) wireless communications networks [1], [2]. In particular, large-scale antenna arrays at base stations (BSs) or femtocells APs allow to smartly direct the power flux towards intended users thus increasing data rates, whereas mm-wave communication provides a less crowded and larger spectrum [3]–[5].

In next years, it is expected that personal devices localization and communication capabilities will play a crucial

role [6]: in fact, the possibility of localizing nodes in indoor environments will be an essential feature of future devices. In this context, the AP could be used as a single-anchor node, i.e., a node whose position is *a-priori* known, in a radio-localization perspective permitting the mobile users to be aware of their own position. Furthermore, the adoption of more than one antenna at the transmitter (Tx) and receiver (Rx), will enable the user orientation estimation at an accuracy higher than that provided by compass and gyroscopes. Such feature could play a key role in applications beyond 5G as for example augmented reality and simultaneous localization and mapping (SLAM), where trajectory errors, comprising both position and orientation estimation inaccuracies, dramatically affect the performance [7]. Contrarily to traditional scenarios where dedicated multiple anchor nodes are necessary to allow classic triangulation/multilateration techniques [8], here the possibility to centralize both communication and localization capabilities in a single multi-antenna AP working at mm-wave frequencies is envisioned with the advantage of drastically decreasing the overall system complexity and cost. Moreover, when operating at such high frequencies, not only APs but also user terminals could adopt massive arrays thanks to the reduced wavelength [9], thus increasing even more the localization accuracy given the potential huge set of measurements [10]–[13].

While at microwave frequencies the antenna array technology is quite mature, at mm-wave severe technological constraints are still present and must be taken into account when designing positioning systems. Recently, massive antennas prototypes have been proposed with electronic beamsteering capabilities. In order to reduce the complexity, they adopt simple switches and thus, the resulting non-perfect signals phasing operations could impact the array radiation characteristics [14]–[16]. In such a scenario, it becomes of great interest to understand the fundamental limits on localization error with massive antenna arrays both at AP and mobile terminals using only a single reference node.

Concerning the ultimate localization performance evaluation, a rich literature has been produced for the analysis of wideband multiple anchors systems. Specifically, in [17], [18] authors explore the localization accuracy for a wideband sensors network composed of several independent anchors. Their results are further discussed in [19] where a more realistic Rx architecture able to exploit the carrier phases information has been taken in consideration while deriving the localization performance. Differently from these works,

Anna Guerra and Davide Dardari are with the Dipartimento di Ingegneria dell'Energia Elettrica e dell'Informazione "Guglielmo Marconi" - DEI, University of Bologna, via Venezia 52, 47521 Cesena, ITALY.

(e-mail: anna.guerra3@unibo.it, davide.dardari@unibo.it).

Francesco Guidi is with CEA, LETI, MINATEC Campus, 38054 Grenoble, France. (e-mail: francesco.guidi@cea.fr).

This research was supported in part by the XCycle project (Grant 635975) and by the IF-EF Marie-Curie project MAPS (Grant 659067). Authors would like to thank Nicolò Decarli, Raffaele D'Errico and Henk Wymeersch for fruitful discussions.

where anchors send orthogonal waveforms, we consider a signal model dependent on the particular arrays architecture chosen where both orthogonal and non-orthogonal waveforms can be transmitted. Moreover, our work is not focused on a specific Rx structure, as in [19], but it aims to compare different Tx array architectures. In [20], [21], a joint delay-angle estimation is reported considering different array technologies and frequency bandwidths. Nevertheless, these works analyze the performance in terms of CRB on delay and angular information rather than directly on localization, and neither a comparison between different array schemes, nor the time synchronization issue and the impact of multipath are treated. In our previous work [12], [22], some preliminary results on positioning accuracy considering only beamforming strategies have been presented, but the comparison with multiple-input multiple-output (MIMO), as well as the impact of multipath components (MPCs), was not considered.

Stimulated by this framework, in this paper we conduct a CRB-based analysis of a localization system exploiting the next 5G technologies potentialities. Differently from the state-of-the-art, we adopt a 1-step approach in which the Tx position and orientation are directly inferred from the received signals and, thus, without the need of estimating intermediate parameters (e.g., time-of-arrival (TOA)-direction-of-arrival (DOA)) or applying geometrical methods which do not ensure the optimality of the approach [23].

The main contributions of this work can be summarized as follows:

- Derivation of the theoretical performance limits on the localization and orientation error for different array configurations in a single-anchor scenario;
- Proposal of a signal model valid for any antenna array geometry, configuration (i.e., MIMO, phased, timed arrays), and frequency band. As a case study, in the numerical results the focus is on the adoption of mm-wave massive arrays due to their expected attractiveness in next 5G applications;
- Introduction of low-complexity random weighting approach, i.e., randomly chosen beamforming weights, and analysis of its performance compared to that of classical beamforming and MIMO solutions;
- Investigation of the CRB tightness in massive array regime (i.e., letting the number of antennas $\rightarrow \infty$) for any signal-to-noise ratio (SNR) condition;
- Analysis of the *trade-off* between SNR enhancement obtained via beamforming and diversity gain of MIMO considering the impact of different types of uncertainties, as, for example, the MPCs, beamforming weights and time synchronization errors;
- Demonstration that in the massive array regime (i.e., array antennas $\rightarrow \infty$), the effect of multipath can be made negligible on average.

The rest of the paper is organized as follows. Sec. II describes the geometry of the localization system. Then, Sec. III introduces the signal model taking into account different array structures. In Sec. IV the localization performance limits derivation is reported. Sec. V analyzes the asymptotic

conditions for which the CRB can be considered a tight bound. Sec. VI derived compact formulas for a ideal free-space case. The multipath impact on localization performance are investigated in Sec. VII. Finally, Sec. VIII presents the localization performance results and Sec. IX concludes the work.

Notation: Lower case and capital letters in bold denote vectors and matrices, respectively. The subscripts $[\cdot]^T$, $[\cdot]^*$ and $[\cdot]^H$ indicate the transpose, the conjugate and the Hermitian operators. $\|\cdot\|_2$ is the Euclidean norm, $\mathbf{A} \succeq \mathbf{B}$ indicates that the matrix $\mathbf{A} - \mathbf{B}$ is non-negative definite, and $\text{diag}(\cdot)$ represents the diagonal operator. The subscripts $(\cdot)^t$ and $(\cdot)^r$ refer to quantities related to the transmitting and receiving array, respectively, while the subscript $(\cdot)^{tr}$ to elements that can be referred to both the Tx and the Rx. $(\cdot)^{FS}$ indicates the free-space scenario. $\mathcal{F}(\cdot)$ denotes the Fourier transform operation, $\mathcal{U}(a, b)$ a uniform distribution in the interval $[a, b]$, and $\mathcal{CN}(\mu, \sigma^2)$ a circularly symmetric Gaussian distribution with mean μ and variance σ^2 .

The notations of frequently-used symbols are listed as follows.

N_{tx}, N_{rx}	Number of Tx-Rx array antennas
L	Number of MPCs
A^t, A^r	Area of the Tx-Rx array
$\mathbf{p}^t, \boldsymbol{\vartheta}^t$	Tx centroid position and orientation
$\mathbf{p}^r, \boldsymbol{\vartheta}^r$	Rx centroid position and orientation
d	Distance between Tx-Rx centroids
$S = A^r/d^2$	Ratio between the Rx array area and the squared inter-array distance
$\mathbf{p}_i^t, \mathbf{p}_m^r$	Tx/Rx antenna position
d_{ant}	Inter-antenna spacing
$\mathbf{d}(\boldsymbol{\theta})$	Direction cosine
$\boldsymbol{\kappa}$	Multipath parameters vector
$\boldsymbol{\theta}_1$	Direct path wave direction
$\boldsymbol{\theta}_l$	l th path wave direction
$\boldsymbol{\theta}_0$	Steering direction
τ_{im1}, τ_{iml}	Propagation delay relative to the direct and l th path between the i th Tx- m th Rx antenna
τ_1, τ_l	Propagation delay relative to the direct and l th path between centroids
a_1, α_l	Direct path amplitude and l th complex channel coefficient
$\tau_i^t(\boldsymbol{\theta}_i^t, \boldsymbol{\vartheta}^t)$	Inter-antenna delay between the i th Tx antenna and the relative array centroid
$\tau_m^r(\boldsymbol{\theta}_m^r, \boldsymbol{\vartheta}^r)$	Inter-antenna delay between the m th Rx antenna and the relative array centroid
f_c, W, β	Transmitted signal carrier frequency, bandwidth, baseband effective bandwidth
T_{obs}	Observation interval
E_{tot}, E	Total and normalized energy at each antenna element
N_0	Single-side noise power spectral density
N_F	Receiver noise figure
SNR_1	SNR relative to the direct path
$S_i(f), \mathbf{s}(f)$	Equivalent low-pass signal at the i th Tx antenna and transmitted signals vector in the frequency domain

$P_i(f)$	Equivalent low-pass unitary-energy signal at the i th Tx antenna in the frequency domain
$R_m(f), \mathbf{r}(f)$	Received signal at the m th Rx antenna and received signals vector in the frequency domain
$X_m(f), \mathbf{x}(f)$	Useful Rx signal at the m th Rx antenna and useful Rx signals vector in the frequency domain
$N_m(f), \mathbf{n}(f)$	Noise component at the m th Rx antenna and noise vector in the frequency domain
$\omega_i, \mathbf{B}(f, \boldsymbol{\theta}_0)$	Beamforming weight and matrix
$\mu_i^t(\boldsymbol{\theta}_0), \tau_i^t(\boldsymbol{\theta}_0), \nu_i$	Beamforming phase, TDL and random weight
$\delta_i^t, \Delta\tau_i^t$	Beamforming phase and TDL errors
$\tilde{\omega}_i, \mathbf{Q}(f)$	Beamforming weight and matrix with errors
ϵ^s	Time synchronization error
$\boldsymbol{\psi}$	Estimation parameter vector
$\mathbf{J}_{\boldsymbol{\psi}}, \mathbf{J}_{\boldsymbol{\psi}}^d, \mathbf{J}_{\boldsymbol{\psi}}^p$	Bayesian FIM, FIM relative to data, a -priori FIM
CRB(\mathbf{q})	CRB on position and orientation
CRB ₀	Single-antenna CRB on ranging error

II. ANTENNA ARRAY GEOMETRIC CONFIGURATION

A. Geometric Relationships

We consider a 3D localization scenario, as the one reported in Fig. 1, consisting of a single AP acting as reference receiving node equipped with an antenna array, with N_{rx} antennas, and a transmitting mobile terminal with a N_{tx} -antenna array. The localization process aims at directly inferring:¹

- the position of the Tx centroid $\mathbf{p}^t = [x_0^t, y_0^t, z_0^t]^T = [x, y, z]^T$;
- the orientation of the Tx $\boldsymbol{\vartheta}^t = [\vartheta^t, \varphi^t]^T$

when the Rx centroid position $\mathbf{p}^r = [x_0^r, y_0^r, z_0^r]^T = [0, 0, 0]^T$ and orientation $\boldsymbol{\vartheta}^r = [\vartheta^r, \varphi^r]^T$ are known.² With reference to Fig. 1, $\mathbf{p}_i^t(\boldsymbol{\vartheta}^t) = [x_i^t, y_i^t, z_i^t]^T$ indicates the position of the i th transmitting antenna relative to the Tx geometric center and dependent on the Tx orientation, and $\mathbf{p}_m^r(\boldsymbol{\vartheta}^r) = [x_m^r, y_m^r, z_m^r]^T$ the position of the m th receiving antenna relative to the Rx geometric center. Considering spherical coordinates, we have

$$\mathbf{p}_{i/m}^{\text{tr}}(\boldsymbol{\vartheta}^{\text{tr}}) = \rho_{i/m}^{\text{tr}} \mathbf{R}(\boldsymbol{\vartheta}^{\text{tr}}) \mathbf{d}^{\text{tr}}(\boldsymbol{\theta}_{i/m}^{\text{tr}}) \quad (1)$$

with the direction cosine is expressed as

$$\mathbf{d}(\boldsymbol{\theta}) = [\sin(\theta) \cos(\phi), \sin(\theta) \sin(\phi), \cos(\theta)] \quad (2)$$

and $\rho_{i/m}^{\text{tr}} = \|\mathbf{p}_{i/m}^{\text{tr}}(\boldsymbol{\vartheta}^{\text{tr}}) - \mathbf{p}^{\text{tr}}\|_2$ and $\boldsymbol{\theta}_{i/m}^{\text{tr}} = [\theta_{i/m}^{\text{tr}}, \phi_{i/m}^{\text{tr}}]^T$ being the distance and the couple of angles between the con-

¹ As previously stated, we consider the Tx position and orientation with respect to the relative centroid (see (1)-(3) in the following) as we adopt a 1-step approach in which the Tx position and orientation are directly inferred from the received signals. Thus, we do not estimate neither the DOA (i.e., angle between arrays centroids) nor the direct path TOA.

² Without loss of generality, the Rx is assumed located at the origin of the coordinates system.

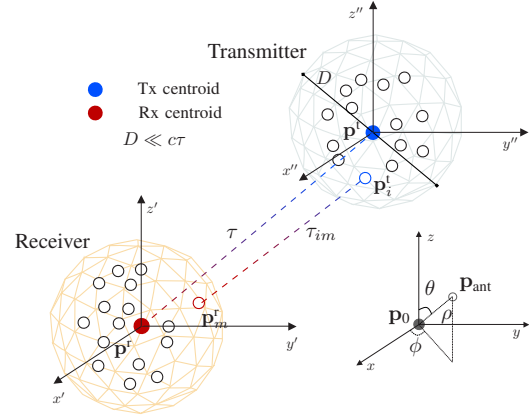


Fig. 1. Multi-antenna system configuration.

sidered array antenna from the correspondent array centroid.³ The rotational matrix $\mathbf{R}(\boldsymbol{\vartheta}^{\text{tr}})$ is given by

$$\mathbf{R}(\boldsymbol{\vartheta}^{\text{tr}}) = \mathbf{R}_z(\varphi^{\text{tr}}) \mathbf{R}_x(\vartheta^{\text{tr}}) \quad (3)$$

where $\mathbf{R}_z(\varphi^{\text{tr}})$ and $\mathbf{R}_x(\vartheta^{\text{tr}})$ define the counter-clock wise rotation around the z -axis and the clock wise rotation around the x -axis, respectively. Finally $\boldsymbol{\theta}_1 = [\theta_1, \phi_1]^T$ designates the angle of incidence between arrays centroids (direct path) and $\boldsymbol{\theta}_0 = [\theta_0, \phi_0]^T$ represents the intended pointing direction of the steering process when applied.

The diameter D of the transmitting and receiving arrays is assumed much smaller than the inter-array distance $d = \|\mathbf{p}^r - \mathbf{p}^t\|_2$, i.e., $D \ll d$. Note that this hypothesis is especially verified at mm-wave where the array dimensions are very small thanks to the reduced wavelength. Moreover the arrays are supposed to be sufficiently far from the surrounding scatterers thus obtaining identical angles of incidence for both direct and MPCs at each antenna element.

We take L MPCs into consideration as nuisance parameters in the localization process and the first path is assumed always experiencing a line-of-sight (LOS) propagation condition. For what the MPCs parameters are concerned, we follow the same notation introduced in [19]. In particular, let $\boldsymbol{\theta}_l^t = [\theta_l^t, \phi_l^t]^T = [\theta_1 + \Delta\theta_l^t, \phi_1 + \Delta\phi_l^t]^T$ and $\boldsymbol{\theta}_l^r = [\theta_l^r, \phi_l^r]^T = [\theta_1 + \Delta\theta_l^r, \phi_1 + \Delta\phi_l^r]^T$, with $l = 1, 2, \dots, L$, indicate the angles of departure from the transmitting array and of incidence at the Rx side of the l th path, respectively. The angular biases $[\Delta\theta_l^t, \Delta\phi_l^t]^T$ and $[\Delta\theta_l^r, \Delta\phi_l^r]^T$ are the displacement with respect to the direct path at the Tx and Rx side. Obviously, it is $[\Delta\theta_1^t, \Delta\phi_1^t]^T = [\Delta\theta_1^r, \Delta\phi_1^r]^T = [0, 0]^T$, when direct path is considered.

Let $\tau_1 \triangleq \|\mathbf{p}^r - \mathbf{p}^t\|_2/c = d/c$ and $\tau_{im1} \triangleq \|\mathbf{p}_m^r - \mathbf{p}_i^t\|_2/c$ being the propagation delay related to the direct path between the transmitting and receiving centroids and between the i th and m th antenna, respectively, where c is the speed of light. Considering the multipath, the l th propagation delay between array centroids is defined as $\tau_l = \tau_1 + \Delta\tau_l$ where $\Delta\tau_l$ is the non-negative delay bias of the l th path with $\Delta\tau_1 = 0$ [19].

³Note that the elevation angle in all the text is indicated with θ and it can assume values in the interval $[0, \pi)$. Contrarily the azimuthal angle is denoted with ϕ and it ranges between $[0, 2\pi)$.

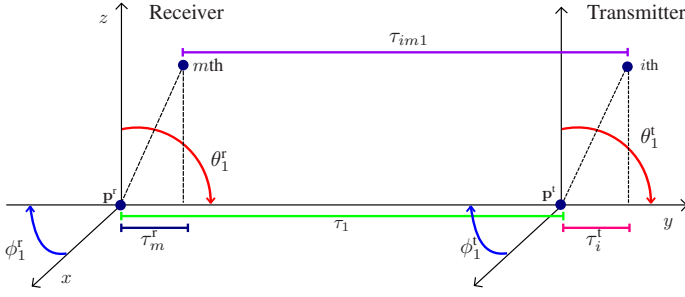


Fig. 2. Array geometric configuration.

According to the geometric assumption previously described, the TOA and amplitude between each couple of transmitting and receiving antennas can be expressed using the following approximations [19], [21]

$$1) \tau_{iml} \approx \tau_l + \tau_i^t(\theta_l^t, \vartheta^t) - \tau_m^r(\theta_l^r, \vartheta^r) \quad 2) a_{iml} \approx a_l \quad (4)$$

where a_{iml} is the amplitude of the l th path between the m th receiving and the i th transmitting antenna, and $\tau_m^r(\theta_l^r, \vartheta^r)$ and $\tau_i^t(\theta_l^t, \vartheta^t)$ are, respectively, the receiving and transmitting inter-antenna propagation delays defined as

$$\tau_{i/m}^{\text{tr}}(\theta_l^{\text{tr}}, \vartheta^{\text{tr}}) = \frac{1}{c} \mathbf{d}(\theta_l^{\text{tr}}) \mathbf{p}_{i/m}^{\text{tr}}(\vartheta^{\text{tr}}) \quad (5)$$

Fig. 2 reports a graphical explanation of the considered system and delays. As it can be seen, the approximation in (4) permits to write the TOA as the summation of the inter-antenna delays and the delay between the array centroids.

B. Special Case: Planar Array Geometry

Planar array configurations appear to be the most suitable when considering the integration of massive arrays in portable devices or in small spaces. For this reason, in addition to the general analysis valid for any geometric configuration (i.e., any antennas spatial deployment and arrays orientation), some compact specialized equations will be derived in the following sections for squared arrays of area $A^t = d_{\text{ant}}^2 N_{\text{tx}}$ ($A^r = d_{\text{ant}}^2 N_{\text{rx}}$), with the antennas equally spaced of d_{ant} . Both arrays are considered lying on the XZ -plane and being located one in front of the other with $\mathbf{p}^r = [0, 0, 0]^T$ and $\mathbf{p}^t = [0, y, 0]^T$ with $y > 0$, so that $d = y$ and thus $\tau_1 = y/c$. In this case, the antenna coordinates in (1) becomes

$$\mathbf{p}_m^{\text{tr}}(\vartheta^{\text{tr}}) = [x_m^{\text{tr}}, 0, z_m^{\text{tr}}]^T = \mathbf{R}(\vartheta^{\text{tr}}) [m_x d_{\text{ant}}, 0, m_z d_{\text{ant}}]^T \quad (6)$$

where $m_x = m_z = -\frac{\sqrt{N-1}}{2}, -\frac{\sqrt{N-1}}{2} + 1, \dots, \frac{\sqrt{N-1}}{2}$ are the antenna indexes along the x - and z -axis respectively, and N indicates the number of antennas.

We assume for now a free-space propagation condition so that $\theta_1^r = \theta_1^t = \theta_1 = [\theta_1, \phi_1]^T = [\frac{\pi}{2}, -\frac{\pi}{2}]^T$ and $\mathbf{d}(\theta_1) = [0, -1, 0]$. Consequently it is possible to specialize (5) as

$$\begin{aligned} \tau_m^r(\theta_1, \vartheta^r) &= -\frac{d_{\text{ant}}}{c} (m_x \sin(\varphi^r) + m_z \cos(\varphi^r) \sin(\vartheta^r)) \\ \tau_i^t(\theta_1, \vartheta^t) &= -\frac{d_{\text{ant}}}{c} (i_x \sin(\varphi^t) + i_z \cos(\varphi^t) \sin(\vartheta^t)) \end{aligned} \quad (7)$$

Note that, in the special case in which the Rx and Tx orientation is $\vartheta^r = \vartheta^t = [0, 0]^T$, the inter-antenna delays

are zeros, i.e. $\tau_m^r(\theta_1, \vartheta^r) = \tau_i^t(\theta_1, \vartheta^t) = 0 \quad \forall m, i$, as the antennas are aligned to the array centroids, thus the incident wave impinges simultaneously at all the antennas.

III. ANTENNA ARRAY SCHEMES AND SIGNAL MODEL

In this section, different types of antenna array schemes are analyzed starting from a unified signal model with the purpose to highlight their beamforming and diversity gain properties. Specifically, the four array structures reported in Fig. 3 will be analysed from a signal processing point-of-view and by focusing on how the different signaling schemes translate into different localization capabilities. Table I reports a comparison in terms of arrays complexity, capabilities and cost.

A. Transmitted Signal Model

The transmitted signal at the i th transmitting antenna is denoted with $g_i(t) = \Re\{s_i(t) e^{j2\pi f_c t}\}$ where $s_i(t)$ represents the equivalent low-pass signal and f_c the carrier frequency. We consider a constraint on the total transmitted energy E_{tot} which is uniformly allocated among antennas, thus $E = E_{\text{tot}}/N_{\text{tx}} = \int_{T_{\text{obs}}} |s_i(t)|^2 dt$, $i = 1, 2, \dots, N_{\text{tx}}$, represents the normalized energy at each antenna element. We introduce the Fourier transform of $s_i(t)$ as $S_i(f) = \mathcal{F}\{s_i(t)\}$, with $\mathcal{F}\{\cdot\}$ denoting the Fourier transform operation in a suitable observation interval T_{obs} containing the signal support. For further convenience, the vector $\mathbf{s}(f) = [S_1(f), \dots, S_{N_{\text{tx}}}(f)]^T$ contains all the baseband transmitted signals. In the following, the signal model for each array configuration will be further detailed with reference to Fig. 3.

1) *Timed and phased arrays*: In multi-antenna systems, beamforming is obtained by applying a progressive time delay at each array element so that the emitted signals result summed up coherently towards the intended steering direction. Considering the signal bandwidth W , when the condition $W \ll f_c$ holds, this process can be well approximated using only phase shifters (PSs) (phased arrays). On the contrary, when $W \approx f_c$, phase shifts are no longer sufficient to align all the signals. As a consequence, to avoid distortion and beamsteering⁴ degradation (squinting effect), timed arrays consisting of PSs and time delay lines (TDLs) must be introduced. The following analysis considers both array structures in order to preserve the generality of the model. Nevertheless, in Sec. VIII, arrays operating at mm-wave frequencies with $W \ll f_c$ (narrowband) will be adopted in simulations.⁵ In [12], different fractional bandwidths have been taken into account in the results.

Moreover, differently from [24], [25], where multiple beams are generated, here we consider a single-beam scenario in order to maximize the SNR in the desired steering direction and to reduce the processing time.

Given these array schemes, the transmitted signal is the same for all transmitting antennas, i.e., $s_i(t) = s(t) = \sqrt{E} p(t) \quad \forall i = 1, \dots, N_{\text{tx}}$, with $p(t)$ being the unitary energy normalized version of $s(t)$, and beamforming weights are applied to each branch of the array to focus the power flux in

⁴The terms beamsteering and beamforming are used as synonymous.

⁵As expected, since $W \ll f_c$, the localization performance of timed and phased arrays coincides.

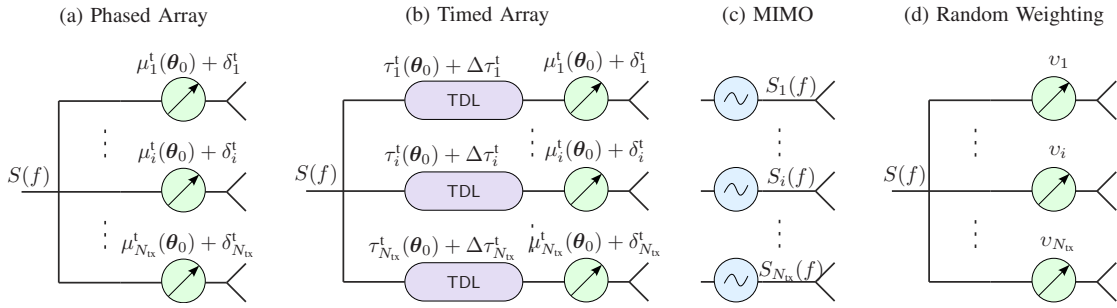


Fig. 3. From the left to the right: Phased, timed, MIMO and random weighting array schemes.

TABLE I
ARRAY SCHEMES COMPARISON.

Signal Design	Array Implementation Complexity	Cost	Beamforming capabilities	
Timed	Low: same signal for all antenna branches	High: TDLs needed when $W \gg f_c$	High	Yes
Phased	Low: same signal for all antenna branches	Medium: only PSs	Medium	Yes
MIMO	High: one different signal for all antenna branches	High: a RF chain for each branch	High	No
Random	Low: same signal for all antenna branches	Low: only PSs	Low	No

a precise direction in space. Specifically, when no quantization errors are present in the weights, the ideal beamforming matrix can be defined as

$$\mathbf{B}(f, \boldsymbol{\theta}_0) = \text{diag}(\omega_1, \omega_2, \dots, \omega_i, \dots, \omega_{N_{\text{tx}}}). \quad (8)$$

The i th beamforming weight is $\omega_i = b_i(f) b_i^c$ having indicated $b_i(f) = e^{j2\pi f \tau_i^t(\boldsymbol{\theta}_0)}$ and $b_i^c = e^{j\mu_i^t(\boldsymbol{\theta}_0)}$, where $\mu_i^t(\boldsymbol{\theta}_0) = 2\pi f_c \tau_i^t(\boldsymbol{\theta}_0)$ and $\tau_i^t(\boldsymbol{\theta}_0)$ are the transmitting steering phase and delay related to the i th PS and TDL of the array, respectively. The main difference between phased and timed array is the way in which the beamsteering process is performed: in the former only PSs are present (i.e., $\tau_i^t(\boldsymbol{\theta}_0) = 0 \forall i = 1, \dots, N_{\text{tx}}$, refer to Fig. 3-(a)) while in the latter TDLs and PSs are both employed to counteract the beamsquinting effect caused by a larger W/f_c ratio (see Fig. 3-(b)). Nevertheless, some technological issues could induce errors in the beamforming vector. Firstly, when digitally controlled PSs are used in place of their high-resolution analog counterparts, the presence of quantization errors has to be accounted for [7]. As shown in [14], [15], where some massive arrays prototypes working in the X- and V-bands have been proposed, PSs can be realized by simply adopting switches, or by rotating patch antennas. Therefore, continuous phase shifts ranging from 0° to 360° are not realizable in practice and the quantization errors generated by the consequent discretization of phases should be taken into account when considering real massive arrays. Secondly, time synchronization between the Tx and the Rx is required to estimate the position. There are several techniques to accomplish this task [26], with the two-way ranging being one of the most used. Unfortunately due to several factors such as clock drift, a residual time synchronization error is always present and it is accounted by the term ϵ^s in our

model. In the presence of such non-perfect weights and time synchronization error, a matrix accounting for all the non-idealities is introduced

$$\mathbf{Q}(f) = e^{-j2\pi(f+f_c)\epsilon^s} \text{diag}(\varsigma_1, \varsigma_2, \dots, \varsigma_i, \dots, \varsigma_{N_{\text{tx}}}) \quad (10)$$

where ς_i takes into account the i th beamforming weight quantization error, i.e., $\varsigma_i = e^{j(2\pi f \Delta\tau_i^t + \delta_i^t)}$ with δ_i^t being the phase error and $\Delta\tau_i^t$ the TDL error. For further convenience, let indicate with $\tilde{\omega}_i = \tilde{b}_i(f) \tilde{b}_i^c$ where $\tilde{b}_i(f) = e^{j2\pi f (\tau_i^t(\boldsymbol{\theta}_0) + \Delta\tau_i^t)}$ and $\tilde{b}_i^c = e^{j(\mu_i^t(\boldsymbol{\theta}_0) + \delta_i^t)}$ the quantized weights. After the transmitting beamforming process, the signal at each antenna element can be written as $\mathbf{Q}(f) \mathbf{B}(f, \boldsymbol{\theta}_0) \mathbf{s}(f)$.

2) *MIMO arrays*: Contrarily to timed or phased arrays, which perform accurate beamforming, MIMO arrays take advantage of the diversity gain provided by multiple different waveforms [27], [28] (see Fig. 3-(c)).⁶ To make the Rx able to discriminate the signal components coming from each single transmitting antenna, orthogonal waveforms are typically adopted [28]–[31]. As an example, in [28] a class of signals (i.e., frequency spread signals) are demonstrated to maintain orthogonality for time delays and frequency Doppler shifts. This comes at the expense of a large bandwidth or symbol duration time and of a higher complexity. In MIMO arrays, the normalized baseband transmitted signals are indicated with $P_i(f) = \mathcal{F}\{p_i(t)\} = \frac{1}{\sqrt{E}} \mathcal{F}\{s_i(t)\}$, where $\int_{T_{\text{obs}}} |p_i(t)|^2 dt = 1, i = 1, 2, \dots, N_{\text{tx}}$. We consider orthogonal waveforms, such

⁶ Note that here we refer to MIMO as done in radar literature rather than in communications.

$$\mathbf{r}(f) = \sum_{l=1}^L \mathbf{a}^{\text{r}}(f, \boldsymbol{\theta}_l^{\text{r}}, \boldsymbol{\vartheta}^{\text{r}}) \mathbf{c}(f, \tau_l) \mathbf{A}^{\text{t}}(f, \boldsymbol{\theta}_l^{\text{t}}, \boldsymbol{\vartheta}^{\text{t}}) \mathbf{Q}(f) \mathbf{B}(f, \boldsymbol{\theta}_0) \mathbf{s}(f) + \mathbf{n}(f) = \mathbf{x}(f) + \mathbf{n}(f) \quad (9)$$

that the correlation function is

$$R_p(\Delta\tau_{ij}^{(l,k)}) = \int_W P_i(f) P_j^*(f) e^{-j2\pi f \Delta\tau_{ij}^{(l,k)}} df = \begin{cases} 0 & i \neq j \\ \neq 0 & i = j \end{cases} \quad \forall l, k = 1, \dots, L \quad (11)$$

where $\Delta\tau_{ij}^{(l,k)} = \tau_{iml} - \tau_{jmk}$ with $m = 1, \dots, N_{\text{rx}}$ and $i, j = 1, \dots, N_{\text{tx}}$. The possibility to provide orthogonal waveforms permits to increase the diversity gain, as it will be detailed in next sections, but it requires a greater bandwidth demand and a more complex Tx structure. In MIMO, the matrix in (8) is an identity matrix $\mathbf{B}(f, \boldsymbol{\theta}_0) = \mathbf{B} = \mathbf{I}_{N_{\text{rx}}}$. In presence of the time synchronization error, (10) becomes $\mathbf{Q}(f) = e^{-j2\pi(f+f_c)\epsilon^s} \mathbf{I}_{N_{\text{rx}}}$.

3) *Random Weighting*: To avoid the complexity of MIMO, we propose a strategy relying on the same structure of phased arrays, i.e., with only PSs at each antenna branch (see Fig. 3-(d)), with the fundamental difference that the value assigned to each PS is randomly chosen. The beamforming matrix of (8) becomes

$$\mathbf{B}(f, \boldsymbol{\theta}_0) = \mathbf{B} = \text{diag}(e^{jv_1}, e^{jv_2}, \dots, e^{jv_i}, \dots, e^{jv_{N_{\text{tx}}}}) \quad (12)$$

with $v_i \sim \mathcal{U}(0, 2\pi)$. Note that in this configuration the matrix in (12) does not depend on the frequency and on the steering direction, thus resulting in an array pattern with a random shape [12]. In the simplest implementation, random weighting could be realized using switches as discrete PSs randomly changing their status [15]. An important aspect is that, for both MIMO and random weighting, the rank of \mathbf{B} is maximum and equal to N_{tx} .

B. Received Signal Model

In this section, a general framework for the received signal model is illustrated. The received signals are collected in a vector $\mathbf{r}(f) = [R_1(f), \dots, R_m(f), \dots, R_{N_{\text{rx}}}(f)]^{\text{T}}$, where $R_m(f) = \mathcal{F}\{r_m(t)\}$ is evaluated in T_{obs} and $r_m(t)$ is the equivalent low-pass received signal at the m th receiving antenna. Specifically, the received signal can be written as in (9). The receiving and transmitting direction matrices for the inter-antennas delays and Tx orientation are given by

$$\mathbf{a}^{\text{r}}(f, \boldsymbol{\theta}_l^{\text{r}}) = [e^{j\gamma_1^{\text{r}}}, \dots, e^{j\gamma_m^{\text{r}}}, \dots, e^{j\gamma_{N_{\text{rx}}}^{\text{r}}}]^{\text{T}} \quad (13)$$

$$\mathbf{A}^{\text{t}}(f, \boldsymbol{\theta}_l^{\text{t}}, \boldsymbol{\vartheta}^{\text{t}}) = \text{diag}(e^{-j\gamma_1^{\text{t}}}, \dots, e^{-j\gamma_i^{\text{t}}}, \dots, e^{-j\gamma_{N_{\text{tx}}}^{\text{t}}}) \quad (14)$$

where $\gamma_{i/m}^{\text{r}} = 2\pi(f+f_c)\tau_{i/m}^{\text{r}}(\boldsymbol{\theta}_l^{\text{r}}, \boldsymbol{\vartheta}^{\text{r}})$; while $\mathbf{c}(f, \tau_l) = c_l \mathbf{1}_{1 \times N_{\text{rx}}}$ is the $1 \times N_{\text{rx}}$ channel vector whose generic element is $c_l = a_l e^{-j2\pi(f+f_c)\tau_l} = \alpha_l e^{-j2\pi f \tau_l}$. Specifically, the dominant LOS component related to direct path (i.e., $l=1$) is considered deterministic while, for $l > 1$, $\alpha_l \sim \mathcal{CN}(0, \sigma_l^2)$ is a circularly symmetric Gaussian random variable (RV)

statistically modelling the l th MPC [32]. Finally, $\mathbf{x}(f) = [X_1(f), \dots, X_m(f), \dots, X_{N_{\text{rx}}}(f)]^{\text{T}}$ is the set of useful received signals and $\mathbf{n}(f) = [N_1(f), \dots, N_m(f), \dots, N_{N_{\text{rx}}}(f)]^{\text{T}}$ is the noise vector with $N_m(f) = \mathcal{F}\{n_m(t)\}$, with $n_m(t) \sim \mathcal{CN}(0, N_0)$ being a circularly symmetric, zero-mean, complex Gaussian noise. For further convenience, define $\nu_t = E_{\text{tot}}/N_0 = \nu N_{\text{tx}}$, with $\nu = E/N_0$. The (total) SNR at each receiving antenna element is $\text{SNR}_t = N_{\text{tx}} \text{SNR}_1$, where $\text{SNR}_1 = (a_1)^2 \nu$ represents the SNR component related to the direct path between a generic couple of TX-RX antenna elements.

IV. POSITION AND ORIENTATION ERROR BOUND

A. Unknown Parameters

The aim of the system is to estimate the position \mathbf{p}^{t} of the Tx and its orientation $\boldsymbol{\vartheta}^{\text{t}}$ starting from the set of received waveforms $\mathbf{r}(f)$.

In this context, MPCs and the residual time synchronization error represent nuisance parameters when evaluating the ultimate performance of the estimator. Thus, the unknown parameters vector is defined as

$$\boldsymbol{\psi} = [\mathbf{q}^{\text{T}}, \boldsymbol{\kappa}^{\text{T}}, \epsilon^{\text{s}}]^{\text{T}} \quad (15)$$

where the parameters of interest related to localization and orientation are collected in $\mathbf{q} = [(\mathbf{p}^{\text{t}})^{\text{T}}, (\boldsymbol{\vartheta}^{\text{t}})^{\text{T}}]^{\text{T}}$, and the multipath parameters in $\boldsymbol{\kappa} = [\boldsymbol{\kappa}_1^{\text{T}}, \boldsymbol{\kappa}_2^{\text{T}}, \dots, \boldsymbol{\kappa}_l^{\text{T}}, \dots, \boldsymbol{\kappa}_L^{\text{T}}]^{\text{T}}$, with

$$\boldsymbol{\kappa}_l = \begin{cases} [a_1]^{\text{T}} & \text{if } l = 1 \\ [\alpha_l^{\text{R}}, \alpha_l^{\text{I}}]^{\text{T}} & \text{if } l > 1. \end{cases} \quad (16)$$

The terms $\alpha_l^{\text{R}} = \Re\{\alpha_l\}$ and $\alpha_l^{\text{I}} = \Im\{\alpha_l\}$ indicate the real and imaginary part of the complex channel coefficient, respectively [33], [34]. The time synchronization error is modeled as independent Gaussian zero-mean RV with standard deviation σ_{ϵ}^2 . Note that the nuisance parameters $\boldsymbol{\psi}_{\text{r}} = [\boldsymbol{\kappa}_2^{\text{T}}, \dots, \boldsymbol{\kappa}_L^{\text{T}}, \epsilon^{\text{s}}]^{\text{T}}$ are described statistically (*a-priori* information available) whereas $\boldsymbol{\psi}_{\text{nr}} = [\mathbf{q}^{\text{T}}, a_1]^{\text{T}}$ are treated as deterministic (no *a-priori* information available).

In the following, we will discern among two different cases based on the orientation awareness. Specifically, we refer to the *orientation-unaware* case for indicating the situation in which the Tx orientation is not known at Rx. Contrarily, the *orientation-aware* case is the opposite situation in which the orientation is exactly known at the Rx side and it can be removed from the list of unknown parameters in (15). Moreover, we suppose that an initial search is conducted by the Tx in order to coarsely estimate its own position and orientation with respect to the Rx. Consequently, the beamforming weights can be communicate to the Rx by exploiting the communication link dedicated to data exchange.

B. CRB General Expression

The performance of any unbiased estimator $\hat{\boldsymbol{\psi}} = \hat{\boldsymbol{\psi}}(\mathbf{r}(f))$ can be bounded by the hybrid CRB defined as [35]

$$\mathbb{E}_{\mathbf{r}, \boldsymbol{\psi}_r} \left\{ \left[\hat{\boldsymbol{\psi}} - \boldsymbol{\psi} \right] \left[\hat{\boldsymbol{\psi}} - \boldsymbol{\psi} \right]^T \right\} \succeq \mathbf{J}_{\boldsymbol{\psi}}^{-1} = \text{CRB}(\boldsymbol{\psi}) \quad (17)$$

where $\mathbf{J}_{\boldsymbol{\psi}}$ is the Bayesian Fisher Information Matrix (FIM) defined as

$$\begin{aligned} \mathbf{J}_{\boldsymbol{\psi}} &\triangleq -\mathbb{E}_{\mathbf{r}, \boldsymbol{\psi}_r} \left\{ \nabla_{\boldsymbol{\psi}}^2 \ln f(\mathbf{r}, \boldsymbol{\psi}_r) \right\} = \mathbf{J}_{\boldsymbol{\psi}}^d + \mathbf{J}_{\boldsymbol{\psi}}^p \\ &= \begin{bmatrix} \mathbf{J}_{\mathbf{q}\mathbf{q}}^d & \mathbf{J}_{\boldsymbol{\kappa}\mathbf{q}}^d & \mathbf{J}_{\boldsymbol{\kappa}\boldsymbol{\kappa}}^d & \mathbf{J}_{\boldsymbol{\kappa}\boldsymbol{\epsilon}^s}^d \\ \mathbf{J}_{\boldsymbol{\kappa}\mathbf{q}}^d & \mathbf{J}_{\boldsymbol{\kappa}\boldsymbol{\kappa}}^d + \mathbf{J}_{\boldsymbol{\kappa}\boldsymbol{\epsilon}^s}^d & \mathbf{J}_{\boldsymbol{\kappa}\boldsymbol{\epsilon}^s}^d & \mathbf{J}_{\boldsymbol{\kappa}\boldsymbol{\epsilon}^s}^d \\ \mathbf{J}_{\boldsymbol{\kappa}\boldsymbol{\kappa}}^d & \mathbf{J}_{\boldsymbol{\kappa}\boldsymbol{\epsilon}^s}^d & \mathbf{J}_{\boldsymbol{\epsilon}^s\boldsymbol{\epsilon}^s}^d + \mathbf{J}_{\boldsymbol{\epsilon}^s\boldsymbol{\epsilon}^s}^p & \mathbf{J}_{\boldsymbol{\epsilon}^s\boldsymbol{\epsilon}^s}^p \end{bmatrix} = \begin{bmatrix} \mathbf{A} & \mathbf{C} \\ \mathbf{C}^H & \mathbf{D} \end{bmatrix}. \end{aligned} \quad (18)$$

The symbol $\nabla_{\boldsymbol{\psi}}^2 = (\partial^2 / \partial \boldsymbol{\psi} \partial \boldsymbol{\psi})$ denotes the second partial derivatives with respect to the elements in $\boldsymbol{\psi}$ and

$$\begin{aligned} \mathbf{J}_{\boldsymbol{\psi}}^d &= -\mathbb{E}_{\mathbf{r}, \boldsymbol{\psi}_r} \left\{ \nabla_{\boldsymbol{\psi}}^2 \ln f(\mathbf{r} | \boldsymbol{\psi}_r) \right\} \\ \mathbf{J}_{\boldsymbol{\psi}}^p &= -\mathbb{E}_{\boldsymbol{\psi}_r} \left\{ \nabla_{\boldsymbol{\psi}}^2 \ln f(\boldsymbol{\psi}_r) \right\} \end{aligned} \quad (19)$$

are the FIM related to data and the FIM containing the *a-priori* statistical information on the parameters, respectively.

Since the observations at each receiving antenna element are independent, the log-likelihood function $\ln f(\mathbf{r} | \boldsymbol{\psi}_r)$ can be written as

$$\ln f(\mathbf{r} | \boldsymbol{\psi}_r) \propto -\frac{1}{N_0} \sum_{m=1}^{N_{\text{rx}}} \int_W |R_m(f) - X_m(f)|^2 df. \quad (20)$$

Moreover, based on the statistical information of $\boldsymbol{\psi}_r$, it is possible to derive the *a-priori* probability density function of parameters $\boldsymbol{\psi}_r$ whose expression is reported in Appendix A. All FIM elements are reported in details in Appendixes A and B.

Finally, by using the Schur complement, the CRB expression related to the localization and orientation estimation error can be easily derived as

$$\text{CRB}(\mathbf{q}) = (\mathbf{A} - \mathbf{C} \mathbf{D}^{-1} \mathbf{C}^H)^{-1}. \quad (21)$$

Equation (21) is a general bound valid for different setup (MIMO, timed, phased and random weighting arrays) and accounting for signal weights quantization effects, time synchronization mismatch and multipath. Specialized expressions can be derived from (21) for specific cases to get insights on the key parameters affecting the performance as will be done in Sec. VI.

V. ON THE CRB TIGHTNESS IN MASSIVE ARRAY REGIME

It is well known that the CRB is a meaningful metric when the global ambiguities are negligible [35]. Such a condition is satisfied when operating at high SNR (asymptotic SNR regime) but, unfortunately, the required high SNRs cannot be in general obtained, especially at high frequencies.

Therefore, in the following, we demonstrate that the global ambiguities can be made negligible without imposing the SNR to be very large by letting the antenna array being massive (*massive array regime*). In particular, we aim to show that, under random Rx array orientations, the number of geometric configurations in which the ambiguities are not negligible

vanishes as the number of receiving antennas increases.

To this purpose, the ambiguity function (AF) is a powerful tool to investigate the presence of ambiguities especially used in radar systems and, it can be derived from the maximum likelihood (ML) discarding the thermal noise component [36]. Let define the normalized AF as

$$\text{AF}(\mathbf{p}, \tilde{\mathbf{p}}) = \left| \frac{T_{\text{obs}}}{N_{\text{tx}} N_{\text{rx}}} \int_W \mathbf{x}^H(f, \mathbf{p}) \mathbf{x}(f, \tilde{\mathbf{p}}) df \right|^2 \quad (22)$$

where \mathbf{p} is the true Tx position, $\tilde{\mathbf{p}}$ is a test position and, \mathbf{x} is the useful signal vector reported in (9). Asymptotically for $N_{\text{rx}} \rightarrow \infty$ (*massive array regime*), for the weak law of the large number [37], we can write

$$\text{AF}(\mathbf{p}, \tilde{\mathbf{p}}) \xrightarrow{P} \left| \frac{T_{\text{obs}}}{N_{\text{tx}} N_{\text{rx}}} \int_W \mathbb{E}[\mathbf{x}^H(f, \mathbf{p}) \mathbf{x}(f, \tilde{\mathbf{p}})] df \right|^2 \quad (23)$$

where the operator \xrightarrow{P} indicates the convergence in probability. In the following, we will consider the free-space and the multipath cases, separately, in order to show how the sidelobes level behaves in the massive array regime. The analysis in non-massive array regime is considered in Sec. VIII.

A. Free-space Scenario

Here we focus our attention to the free-space scenario (i.e., $l = k = 1$). In this case, the expectation term in (23) becomes

$$\frac{1}{N_{\text{tx}} N_{\text{rx}}} \mathbb{E}[\mathbf{x}^H(f, \mathbf{p}) \mathbf{x}(f, \tilde{\mathbf{p}})] \propto \frac{1}{N_{\text{tx}} N_{\text{rx}}} \mathbb{E}[\mathbf{H}(\mathbf{p}, \tilde{\mathbf{p}})] \quad (24)$$

where $\mathbf{H}(\mathbf{p}, \tilde{\mathbf{p}})$, is a $N_{\text{tx}} \times N_{\text{tx}}$ matrix whose generic element is given by

$$\begin{aligned} [\mathbf{H}(\mathbf{p}, \tilde{\mathbf{p}})]_{i,j} &= |a_1|^2 e^{-j 2\pi (f+f_c) \Delta \tau_1(\mathbf{p}, \tilde{\mathbf{p}})} \tilde{\omega}_i \tilde{\omega}_j^* \\ &\times e^{j \Psi_{ij}^{(1,1)}(\mathbf{p}, \tilde{\mathbf{p}})} \sum_{m=1}^{N_{\text{rx}}} \mathbb{E} \left[e^{j \Psi_m^{(1,1)}(\mathbf{p}, \tilde{\mathbf{p}}, \boldsymbol{\vartheta}^r)} \right] \\ &= \begin{cases} |a_1|^2 N_{\text{rx}} e^{j \Psi_{ij}^{(1,1)}(\mathbf{p}, \tilde{\mathbf{p}})} & \mathbf{p} = \tilde{\mathbf{p}} \\ 0 & \text{otherwise} \end{cases} \end{aligned} \quad (25)$$

where we have defined $\Delta \tau_1(\mathbf{p}, \tilde{\mathbf{p}}) = \tau_1(\mathbf{p}) - \tau_1(\tilde{\mathbf{p}})$, $\Psi_{ij}^{(1,1)}(\mathbf{p}, \tilde{\mathbf{p}}) = \gamma_i^t(\mathbf{p}, \boldsymbol{\vartheta}^t) - \gamma_j^t(\tilde{\mathbf{p}}, \boldsymbol{\vartheta}^t)$ and $\Psi_m^{(1,1)}(\mathbf{p}, \tilde{\mathbf{p}}, \boldsymbol{\vartheta}^r) = -\gamma_m^r(\mathbf{p}, \boldsymbol{\vartheta}^r) + \gamma_m^r(\tilde{\mathbf{p}}, \boldsymbol{\vartheta}^r)$ which depends on the Rx array orientation. Note that $\Psi_m^{(1,1)}(\mathbf{p}, \tilde{\mathbf{p}}, \boldsymbol{\vartheta}^r) = 0$ for $\mathbf{p} = \tilde{\mathbf{p}}$ regardless the Rx orientation. On the other side, when $\mathbf{p} \neq \tilde{\mathbf{p}}$, in the presence of a large number of antenna elements ($N_{\text{rx}} \rightarrow \infty$) and considering random Rx orientations, the inter-antenna phase terms $\Psi_m(\mathbf{p}, \tilde{\mathbf{p}}, \boldsymbol{\vartheta}^r)$ can be modeled as independent RVs uniformly distributed in $[0, 2\pi)$. In fact, different geometric configurations permit to span all the angles especially when large arrays are considered ⁷.

This means that the percentage of geometrical configurations of the Rx for which the ambiguities are not negligible (i.e., $\text{AF}(\mathbf{p}, \tilde{\mathbf{p}}) \rightarrow 0$ when $\mathbf{p} \neq \tilde{\mathbf{p}}$), vanishes as N_{rx} increases.

In other words, the conditions that permit to operate in the non-ambiguity region during the CRB evaluation are twofold:

⁷The goodness of the fitting with a uniform distribution has been validated through simulations.

the first is to increase the SNR (high-SNR regime) by keeping the number of antennas fixed, whereas the second fixes the SNR (even not extremely large) and let the number of antennas explode.

B. Multipath Scenario

This section aims at investigating if the CRB still remains a meaningful metric in the presence of multipath. To this purpose, we consider the normalized AF by putting in evidence the multipath contribution, as

$$\begin{aligned} \text{AF}(\mathbf{p}, \tilde{\mathbf{p}}) &= \left| \frac{T_{\text{obs}}}{N_{\text{tx}} N_{\text{rx}}} \int_W \mathbf{x}^{\text{H}}(f, \mathbf{p}) \mathbf{x}(f, \tilde{\mathbf{p}}) df \right|^2 \\ &= \left| \frac{T_{\text{obs}}}{N_{\text{tx}} N_{\text{rx}}} \int_W (\mathbf{x}_1(f, \mathbf{p}) + \mathbf{x}_{l>1}(f, \mathbf{p}))^{\text{H}} \right. \\ &\quad \left. \times (\mathbf{x}_1(f, \tilde{\mathbf{p}}) + \mathbf{x}_{l>1}(f, \tilde{\mathbf{p}})) df \right|^2 \\ &= \left| \int_W \frac{f_{\text{AWGN}}(\mathbf{p}, \tilde{\mathbf{p}})}{N_{\text{tx}} N_{\text{rx}}} + \frac{f_{\text{MP}}(\mathbf{p}, \tilde{\mathbf{p}})}{N_{\text{tx}} N_{\text{rx}}} df \right|^2 \end{aligned} \quad (26)$$

where $\mathbf{x}_1(f, \mathbf{p})$ and $\mathbf{x}_{l>1}(f, \mathbf{p})$ indicate the expected received (noise-free) signal due to the direct path and multipath, respectively. Given the expression in (26), the following asymptotic analysis aims at verifying that the number of times the multipath impacts on the AF shape is negligible compared to the number of times it has not an effect at all, provided that the number of Rx antennas goes to infinity and that random array orientations are considered. More precisely, recalling the weak law of the large numbers, it is

$$\frac{f_{\text{MP}}(\mathbf{p}, \tilde{\mathbf{p}})}{N_{\text{tx}} N_{\text{rx}}} \xrightarrow{P} \frac{1}{N_{\text{tx}} N_{\text{rx}}} \mathbb{E}[f_{\text{MP}}(\mathbf{p}, \tilde{\mathbf{p}})] \quad (27)$$

where we aim at verifying that the right-hand side of (27) is 0 for $\mathbf{p} \neq \tilde{\mathbf{p}}$, meaning that AF sidelobes depending on multipath disappear when N_{rx} is large and random orientations are considered.

The expectation argument in (27) is given by

$$\begin{aligned} \mathbb{E}[f_{\text{MP}}(\mathbf{p}, \tilde{\mathbf{p}})] &= \mathbb{E}[\mathbf{x}_{l>1}^{\text{H}}(f, \mathbf{p}) \mathbf{x}_1(f, \tilde{\mathbf{p}})] \\ &\quad + \mathbb{E}[\mathbf{x}_1^{\text{H}}(f, \mathbf{p}) \mathbf{x}_{l>1}(f, \tilde{\mathbf{p}})] \\ &\quad + \mathbb{E}[\mathbf{x}_{l>1}^{\text{H}}(f, \mathbf{p}) \mathbf{x}_{l>1}(f, \tilde{\mathbf{p}})]. \end{aligned} \quad (28)$$

Treating separately the terms in (28), we have

$$\begin{aligned} \mathbb{E}[\mathbf{x}_1^{\text{H}}(f, \mathbf{p}) \mathbf{x}_{l>1}(f, \tilde{\mathbf{p}})] &= \\ &= \sum_{mij} \sum_{k=2}^L \alpha_k^* \alpha_k S_i(f) S_j^*(f) \tilde{\omega}_i \tilde{\omega}_j^* e^{-j2\pi f \tau_k} e^{-j \Psi_{ij}^{(1,k)}(\mathbf{p}, \tilde{\mathbf{p}})} \\ &\quad \times \mathbb{E}\left[e^{j \Psi_m^{(1,k)}(\mathbf{p}, \tilde{\mathbf{p}})}\right] = 0 \quad \forall \tilde{\mathbf{p}} \end{aligned} \quad (29)$$

where $\sum_{mij} = \sum_{m=1}^{N_{\text{rx}}} \sum_{i=1}^{N_{\text{tx}}} \sum_{j=1}^{N_{\text{tx}}}$, $\Psi_m^{(1,k)}(\mathbf{p}, \tilde{\mathbf{p}}) = -\gamma_m(\boldsymbol{\theta}_1, \boldsymbol{\vartheta}^r) + \gamma_m(\boldsymbol{\theta}_k, \boldsymbol{\vartheta}^r)$, $\Psi_{ij}^{(1,k)} = -\gamma_i(\boldsymbol{\theta}_1(\mathbf{p})) + \gamma_j(\boldsymbol{\theta}_1(\tilde{\mathbf{p}}))$, and $\mathbb{E}\left[e^{-j(2\pi f \tau_k + \Psi_m^{(1,k)}(\mathbf{p}, \tilde{\mathbf{p}}))}\right] = 0$ as the phases are assumed uniformly distributed between 0 and 2π . Similar

considerations are valid for $\mathbb{E}[\mathbf{x}_{l>1}^{\text{H}}(f, \mathbf{p}) \mathbf{x}_1(f, \tilde{\mathbf{p}})]$. Finally, consider the last term in (28), i.e.

$$\begin{aligned} \mathbb{E}[\mathbf{x}_{l>1}^{\text{H}}(f, \mathbf{p}) \mathbf{x}_{l>1}(f, \tilde{\mathbf{p}})] &= \\ &= \sum_{mij} \sum_{l=2}^L \sum_{k=2}^L S_i(f) S_j(f) \tilde{\omega}_i \tilde{\omega}_j^* e^{-j \Psi_{ij}^{(l,k)}(\mathbf{p}, \tilde{\mathbf{p}})} \\ &\quad \times \alpha_l \alpha_k^* e^{-j2\pi f \Delta\tau_{lk}} \mathbb{E}\left[e^{-j \Psi_m^{(l,k)}(\mathbf{p}, \tilde{\mathbf{p}})}\right] \end{aligned} \quad (30)$$

where $\Delta\tau_{lk} = \tau_l - \tau_k$, $\Psi_m^{(l,k)}(\mathbf{p}, \tilde{\mathbf{p}}) = \gamma_m^r(\boldsymbol{\theta}_l, \mathbf{p}, \boldsymbol{\vartheta}^r) - \gamma_m^r(\boldsymbol{\theta}_k, \tilde{\mathbf{p}}, \boldsymbol{\vartheta}^r)$, $\Psi_{ij}^{(l,k)}(\mathbf{p}, \tilde{\mathbf{p}}) = \gamma_i^l(\boldsymbol{\theta}_l, \mathbf{p}) - \gamma_i^l(\boldsymbol{\theta}_k, \tilde{\mathbf{p}})$. In this case, since it holds

$$\begin{aligned} \mathbb{E}\left[e^{-j \Psi_m^{(l,k)}(\mathbf{p}, \tilde{\mathbf{p}})}\right] &= \begin{cases} 0 & \text{if } l \neq k, \quad \forall \tilde{\mathbf{p}} \\ 1 & \text{if } l = k, \quad \mathbf{p} = \tilde{\mathbf{p}} \\ \mathbb{E}\left[e^{-j \Psi_m^{(l,l)}(\mathbf{p}, \tilde{\mathbf{p}})}\right] = 0 & \text{if } l = k, \quad \mathbf{p} \neq \tilde{\mathbf{p}}, \end{cases} \end{aligned} \quad (31)$$

it follows that (30) is equal to 0 for $\mathbf{p} \neq \tilde{\mathbf{p}}$, i.e. in all those cases in which a global ambiguity can arise.

The obtained result shows that the global ambiguities due to the multipath are, on average, negligible. Nevertheless, the effect of multipath still remains in the correspondence of the true peak of the AF, i.e., that for $\mathbf{p} = \tilde{\mathbf{p}}$, as reported in (31) for $l = k$. Consequently, even if we can state that the CRB is a valid metric in establishing the ultimate performance provided that N_{rx} is sufficiently large, the effect of multipath on the localization accuracy necessitates to be investigated. Specifically, Sec. VII analyzes the effect of multipath from a localization accuracy point-of-view.

VI. FREE-SPACE LOCALIZATION BOUND

Here we provide an example on how the general expression (21) can be simplified in absence of beamforming weights errors and MPCs. Specifically, in free-space conditions, (18) can be reduced to

$$\mathbf{J}_{\psi}^{\text{d}} = \mathbf{J}_{\psi} = \begin{bmatrix} \mathbf{J}_{\mathbf{q}\mathbf{q}} & \mathbf{J}_{\mathbf{q}a_1} \\ \mathbf{J}_{a_1\mathbf{q}} & J_{a_1 a_1} \end{bmatrix} = \begin{bmatrix} \mathbf{J}_{\mathbf{q}\mathbf{q}}^{\text{FS}} & \mathbf{0} \\ \mathbf{0} & J_{a_1 a_1} \end{bmatrix} \quad (32)$$

where its elements are reported in Appendix B and where the superscript ^d is omitted as in this case all the parameters to estimate are deterministic. For readability convenience, we report here the expression of the FIM related to the localization parameters, that is:

$$\begin{aligned} J_{q_b q_a} &= 8\pi^2 \nu a_1^2 \sum_{mij} \Re \left\{ \tilde{b}_{ij}^c \xi_{ij}^{(1,1)} \chi_{ij}^{(1,1)}(2) \right\} \\ &\quad \times \nabla_{q_a}(\tau_{im1}) \nabla_{q_b}(\tau_{jm1}) \end{aligned} \quad (33)$$

where q_a/q_b are two elements in the set $\{x, y, z, \vartheta^l, \varphi^l\}$, and

$$\chi_{ij}^{(1,1)}(2) = \int_W \tilde{b}_{ij}(f) (f + f_c)^2 e^{-j2\pi f \Delta\tau_{ij}^{(1,1)}} P_i(f) P_j^*(f) df \quad (34)$$

with $\Delta\tau_{ij}^{(1,1)} = \tau_{im1} - \tau_{jm1}$, $\xi_{ij}^{(1,1)} = e^{-j2\pi f_c \Delta\tau_{ij}^{(1,1)}}$, $\tilde{b}_{ij}(f) = \tilde{b}_i(f) \tilde{b}_j^*(f)$, and $\tilde{b}_{ij}^\xi = \tilde{b}_i^\xi (\tilde{b}_j^\xi)^*$. In (33), the derivatives translate the TOA and DOA in position and orientation information. In particular, for the position we have

$$\nabla_p(\tau_{im1}) = \frac{1}{c} \left\{ c \nabla_p(\tau_1) + \nabla_p(\boldsymbol{\theta}_1) [\mathbf{p}_i^t(\boldsymbol{\vartheta}^t) - \mathbf{p}_m^r(\boldsymbol{\vartheta}^r)] \right\}. \quad (35)$$

The term $\nabla_p(\tau_1)$ expresses the dependence of the position from the direct path TOA; while

$$\begin{aligned} \nabla_p(\boldsymbol{\theta}_1) = & \nabla_p(\theta_1) \cos(\theta_1) \begin{bmatrix} \cos(\phi_1) \\ \sin(\phi_1) \\ -\tan(\phi_1) \end{bmatrix}^T \\ & + \nabla_p(\phi_1) \sin(\theta_1) \begin{bmatrix} -\sin(\phi_1) \\ \cos(\phi_1) \\ 0 \end{bmatrix}^T \end{aligned} \quad (36)$$

includes the dependence of the position from the DOA information. Finally, for what the orientation information is regarded, we have

$$\nabla_{\boldsymbol{\vartheta}^t}(\tau_{im1}) = \nabla_{\boldsymbol{\vartheta}^t}(\tau_i^t(\boldsymbol{\theta}_1, \boldsymbol{\vartheta}^t)) = \frac{1}{c} \mathbf{d}(\boldsymbol{\theta}_1) \nabla_{\boldsymbol{\vartheta}^t}(\mathbf{p}_i^t(\boldsymbol{\vartheta}^t)). \quad (37)$$

By further analyzing (33), one can notice the dependence of the FIM from the beamforming weights given by the coefficients \tilde{b}_{ij}^ξ and $\tilde{b}_{ij}(f)$.

Given the FIM in (33) and starting from (32), it can be easily found that for beamforming and MIMO it is

$$\text{CRB}^{\text{FS}}(\mathbf{q}) = (\mathbf{J}_{\mathbf{q}\mathbf{q}}^{\text{FS}})^{-1} = \left(\check{\mathbf{J}}_{\mathbf{q}\mathbf{q}}^{\text{FS}} \mathbf{G} \right)^{-1} \quad (38)$$

where we have separated the effect of signal design $\check{\mathbf{J}}_{\mathbf{q}\mathbf{q}}^{\text{FS}}$, i.e., that related to (34), from that of the geometry \mathbf{G} , i.e., that related to (35)-(37). Specifically for timed arrays, we have

$$\check{\mathbf{J}}_{\mathbf{q}\mathbf{q}}^{\text{FS}} = 8\pi^2 \text{SNR}_1 (\beta^2 + f_c^2), \quad \mathbf{G} = \sum_{mij} \nabla_{\mathbf{q}\mathbf{q}}(\tau_{im1}, \tau_{jm1}) \quad (39)$$

where $\nabla_{\mathbf{q}\mathbf{q}}(\tau_{im1}, \tau_{jm1})$ is a 5×5 matrix whose entries are given by $\nabla_{q_a}(\tau_{im1}) \nabla_{q_b}(\tau_{jm1})$, and β is the baseband effective bandwidth of $p(t)$, defined as

$$\beta = \left(\int_W f^2 |P(f)|^2 df \right)^{\frac{1}{2}}. \quad (40)$$

Similarly, for MIMO arrays, it is possible to find

$$\check{\mathbf{J}}_{\mathbf{q}\mathbf{q}}^{\text{FS}} = 8\pi^2 \text{SNR}_1 (\beta_i^2 + f_c^2), \quad \mathbf{G} = \sum_{mi} \nabla_{\mathbf{q}\mathbf{q}}(\tau_{im1}, \tau_{im1}) \quad (41)$$

where $\sum_{mi} = \sum_{m=1}^{N_{\text{tx}}} \sum_{i=1}^{N_{\text{rx}}}$ and $\beta_i^2 = \frac{\beta^2}{N_{\text{rx}}}$ is the squared baseband effective bandwidth of $p_i(t)$.

The matrix \mathbf{G} provides, through derivatives, the relationship between the TOA at each TX-RX antenna element couple and the Tx position and orientation.

To improve the comprehension of (38)-(39), in the next sections two particular cases of planar MIMO and timed arrays will be discussed considering a fixed Tx and Rx orientation

i.e., $\boldsymbol{\vartheta}^t = \boldsymbol{\vartheta}^r = [0, 0]^T$. Note that the overall CRB analysis is still valid for any orientation. In Secs. VI-1 and VI-2, we choose a specific case just to provide some insights on how the number of transmitting and receiving antennas can impact the performance. In Appendix C, the matrix \mathbf{G} is evaluated, considering this specific array geometry.

1) *Special Case: Planar MIMO Array:* For the planar geometric configuration and in the *orientation-unaware* case, the diagonal elements in the position and orientation CRB matrix derived starting from (38)-(39) and from (55), are given by

$$\begin{aligned} \text{CRB}(x) = \text{CRB}(z) &= \text{CRB}_0 \frac{12}{S(N_{\text{rx}} - 1)} \\ \text{CRB}(y) &= \frac{\text{CRB}_0}{N_{\text{rx}}} \\ \text{CRB}(\vartheta^t) = \text{CRB}(\varphi^t) &= \text{CRB}_0 \frac{12(N_{\text{tx}} + N_{\text{rx}} - 2)}{A_{\text{rx}}(N_{\text{tx}} - 1)(N_{\text{rx}} - 1)} \end{aligned} \quad (42)$$

where $\text{CRB}_0 = c^2 / (8\pi^2 \text{SNR}_t (\beta_i^2 + f_c^2))$ is the CRB of the ranging error one would obtain using single antenna, and $S = A^r / y^2$ represents the ratio between the Rx array area and the squared Tx-Rx distance. Note that CRB_0 depends on the carrier frequency f_c , on the shape of the pulse through β_i^2 , on the received SNR, and it does not depend on the number of transmitting antennas. The analytical derivation is reported in Appendix C. From (42), it is possible to remark that the CRB of the estimation error in the y -coordinate is inversely proportional to the number of the receiving antenna elements accounting for the number of independent measurements available at the Rx. Regarding the other two coordinates, a key parameter on the estimation accuracy is S which is related to the ratio between the dimension of the Rx array and the distance between the arrays: as this ratio becomes smaller (i.e., as the distance between the arrays becomes larger with respect to the array size), the positioning accuracy degrades. From (42) it is also possible to notice that the accuracy in estimating the orientation depends both on the transmitting and receiving antennas. Specifically both N_{tx} and N_{rx} must be greater than one to make the orientation possible, whereas for the positioning, the constraint is only on the number of receiving elements that must be larger than 1. Moreover, non-zero off-diagonal elements remark a correlation between the error on the estimation of position and orientation. Specifically we have

$$\begin{aligned} \text{CRB}(z, \vartheta^t) = \text{CRB}(\vartheta^t, z) &= \text{CRB}(x, \varphi^t) = \text{CRB}(\varphi^t, x) \\ &= \text{CRB}_0 \frac{12}{S y (1 - N_{\text{rx}})}. \end{aligned} \quad (43)$$

Contrarily in the *orientation aware* case, it can be found

$$\begin{aligned} \text{CRB}(x) = \text{CRB}(z) &= \text{CRB}_0 \frac{12}{S(N_{\text{tx}} + N_{\text{rx}} - 2)} \\ \text{CRB}(y) &= \frac{\text{CRB}_0}{N_{\text{rx}}}. \end{aligned} \quad (44)$$

Note that when passing from a condition of *orientation-unawareness* to that of *orientation-awareness* the positioning

accuracy increases, thanks to the additional information provided. In fact, the CRB on x and z coordinates now depends also on the number of transmitting antennas.

2) *Special Case: Planar Timed Array*: Differently from MIMO, here in the *orientation-unaware* case, the equivalent FIM for position and orientation is singular meaning that it is not possible to jointly localize and determine the orientation using beamforming strategies. Nevertheless, when multiple beams are generated [24], [25], such singularity can be solved thus allowing the localization process, but at the prize of an increased scanning time if the beams are sequentially generated in time, or of a decreased SNR if such beams are simultaneously formed. The investigation of this trade-off is out-of-the-scope of this paper.

If the Tx orientation is a known parameter (*orientation aware* case) and it is discarded from the estimation parameters vector, the elements of the position CRB matrix result from (56)

$$\begin{aligned} \text{CRB}(x) &= \text{CRB}(z) = \text{CRB}_0 \frac{12}{S} \frac{1}{N_{\text{tx}}(N_{\text{tx}} - 1)} \\ \text{CRB}(y) &= \frac{\text{CRB}_0}{N_{\text{tx}} N_{\text{rx}}}. \end{aligned} \quad (45)$$

From (45) it is possible to remark that the CRB of the estimation error in the y -coordinate is inversely proportional to N_{tx} and N_{rx} : in fact, the N_{tx} term accounts for the SNR enhancement due to the beamforming process while the N_{rx} term accounts for the number of independent measurements available at the Rx (receiver diversity). Note that when $N_{\text{rx}} = 1$, the localization along the x and z axes is not possible (only ranging in the y direction), as for MIMO. Refer to Appendix C for more details related to the derivation of (45).

VII. MULTIPATH EFFECT ON LOCALIZATION ACCURACY

Once verified that the CRB is a meaningful metric in different propagation conditions in Sec. V-B, we now investigate the impact of MPCs on the localization performance for the considered scenario. In [18], it is demonstrated that only the information related to the *first-contiguous cluster*, i.e. the set of MPCs overlapped to the first path, is relevant from a localization perspective in the asymptotic SNR regime. Here we show that under the asymptotic massive antenna regime, all the MPCs can be made negligible, included those belonging to the first-contiguous cluster.

The FIM in presence of multipath can be written as follows

$$\mathbf{J}_\psi = \begin{bmatrix} \mathbf{J}_{\mathbf{q}\mathbf{q}} & \mathbf{J}_{\mathbf{q}\boldsymbol{\kappa}} \\ \mathbf{J}_{\boldsymbol{\kappa}\mathbf{q}} & \mathbf{J}_{\boldsymbol{\kappa}\boldsymbol{\kappa}} \end{bmatrix} \quad (46)$$

where $\mathbf{J}_{\boldsymbol{\kappa}\boldsymbol{\kappa}}$ contains also the *a-priori* information on MPCs statistics reported in Appendix A. Consequently, the CRB for the multipath scenario can be formulated as

$$\text{CRB}(\mathbf{q}) = (\mathbf{J}_{\mathbf{q}\mathbf{q}} - \mathbf{J}_{\mathbf{q}\boldsymbol{\kappa}} \mathbf{J}_{\boldsymbol{\kappa}\boldsymbol{\kappa}}^{-1} \mathbf{J}_{\boldsymbol{\kappa}\mathbf{q}})^{-1} \quad (47)$$

where all multipath information is gathered in $\mathbf{J}_{\mathbf{q}\boldsymbol{\kappa}} \mathbf{J}_{\boldsymbol{\kappa}\boldsymbol{\kappa}}^{-1} \mathbf{J}_{\boldsymbol{\kappa}\mathbf{q}}$. Considering the average over different geometric configurations (e.g., the average over different Rx orientations) and for large values of N_{rx} , it is possible to show that the number of configurations where the multipath impacts the localization

performance compared to the number of configurations in which it does not influence the accuracy is negligible regardless the array architecture chosen.

Considering (47), for the weak law of the large number (i.e., for $N_{\text{rx}} \rightarrow \infty$), it holds

$$\frac{1}{N_{\text{rx}} N_{\text{tx}}} \mathbf{J}_{\mathbf{q}\boldsymbol{\kappa}} \xrightarrow{P} \frac{1}{N_{\text{rx}} N_{\text{tx}}} \mathbb{E}[\mathbf{J}_{\mathbf{q}\boldsymbol{\kappa}}] \quad (48)$$

where we aim at demonstrating that

$$\frac{1}{N_{\text{rx}} N_{\text{tx}}} \mathbb{E}[\mathbf{J}_{\mathbf{q}\boldsymbol{\kappa}}] = 0. \quad (49)$$

In the presence of a large number of antenna elements and considering random Rx orientations, the inter-antenna phase terms can be modeled as RVs uniformly distributed in $[0, 2\pi)$. Under this assumption, we have

$$\begin{aligned} \mathbb{E}[J_{q a_1}] &= J_{q a_1} = 0 \\ \mathbb{E}[J_{q \alpha_{ij}^{\Re}}] &= -4 \pi a_1 \nu \sum_{mij} \Im \left\{ \tilde{b}_{ij}^c \mathbb{E} \left[\xi_{ij}^{(k,1)} \chi_{ij}^{(k,1)}(1) \right] \right\} \\ &\quad \times \nabla_q (\tau_{jm1}) = 0 \\ \mathbb{E}[J_{q \alpha_{ij}^{\Im}}] &= 4 \pi a_1 \nu \sum_{mij} \Re \left\{ \tilde{b}_{ij}^c \mathbb{E} \left[\xi_{ij}^{(k,1)} \chi_{ij}^{(k,1)}(1) \right] \right\} \\ &\quad \times \nabla_q (\tau_{im1}) = 0 \end{aligned} \quad (50)$$

where

$$\mathbb{E} \left[\xi_{ij}^{(k,1)} \chi_{ij}^{(k,1)}(1) \right] \propto \mathbb{E} \left[e^{-j 2 \pi (f+f_c) (\Delta \tau_m^r(\boldsymbol{\theta}_1, \boldsymbol{\theta}_k))} \right] = 0 \quad (51)$$

with $\Delta \tau_m^r(\boldsymbol{\theta}_1, \boldsymbol{\theta}_k) = \tau_m^r(\boldsymbol{\theta}_1, \boldsymbol{\vartheta}^r) - \tau_m^r(\boldsymbol{\theta}_k, \boldsymbol{\vartheta}^r)$. Following similar considerations, it is straightforward to prove that the expectation of the $\mathbf{J}_{\boldsymbol{\kappa}\mathbf{q}}$ elements is zero.

The result in (48) leads to the important conclusion that letting the antennas array be massive, i.e., large N_{rx} , makes the set of geometric configurations significantly impacted by MPCs negligible, and the performance converges to that of the free space case. As a consequence, the CRB converges to the CRB averaged over the RX orientations for massive antenna arrays.

VIII. NUMERICAL RESULTS

In this section, numerical results are reported considering different array schemes, multipath conditions and system non-idealities. Four array structures are analyzed: timed arrays equipped with TDLs and PSs, phased and random weighting arrays using only PSs, and finally the MIMO array in which orthogonal waveforms are transmitted and neither PSs nor TDLs are present. For what the antennas spatial deployment is regarded, planar arrays are considered as they represent the most conventional structure to be integrated in APs and mobiles. Differently from Secs. VI-1 and VI-2, here we consider the results averaged over the Rx orientations if not otherwise indicated, and thus it will be possible to appreciate the impact of the array rotational angle on the localization performance. In the following figures, we indicate with \mathbf{Q} the presence of quantization errors, with \mathbf{S} the presence of a residual time synchronization error. Moreover, we designate with:

- *Fixed orientation*: the array configuration with the Tx and the Rx parallel to each other (i.e., $\vartheta^t = \vartheta^r = [0, 0]^T$), as described in Sec. VI;
- *Averaged orientation*: the geometric configuration in which, for each Monte Carlo iteration, a different 3D Rx array orientation is generated, and the CRB is computed as the average over all the partial CRB results computed at each cycle.

Finally, we recall that:

- *Orientation-aware* indicates the case in which the Tx orientation is known at the Rx side and, thus, it is not considered in the parameters vector to be estimated;
- *Orientation-unaware*: the case in which the Tx orientation is unknown at Rx side and it has to be estimated together with the position. In the next figures, we will denote with O , the *orientation-unawareness* case.

A. System Configuration

We consider a scenario with a single AP equipped with a massive array, with the centroid placed in $\mathbf{p}^t = [0, 0, 0]^T$, and a transmitting array antenna whose centroid is located in $\mathbf{p}^r = [0, 5, 0]^T$ ($d = 5$ m).

As in the mathematical model, the Rx has a perfect knowledge of the Tx steering direction, and the results are obtained for $f_c = 60$ GHz and $W = 1$ GHz (the signal duration is $\tau_p = 1.6$ ns) in free-space and multipath conditions. Root raised cosine (RRC) transmitted pulses centered at frequency $f_c = 60$ GHz and roll-off factor of 0.6 are adopted, being compliant with Federal Communications Commission (FCC) mask at 60 GHz [38]. A receiver noise figure of $N_F = 4$ dB and a fixed transmitted power of $P_t = 10$ mW are considered, if not otherwise indicated.

The performance is evaluated in terms of Position Error Bound (PEB) and Orientation Error Bound (OEB) averaged over $N_{\text{cycle}} = 500$ Monte Carlo iterations. For each cycle, a different 3D Rx array orientation, i.e., $\vartheta^r = [\vartheta^r, \varphi^r]^T$, and multipath scenario are generated. Specifically, the receiving (transmitting) antennas are spaced apart of $d_{\text{ant}} = \lambda_L/2$, where $\lambda_L = c/f_L$ and $f_L = f_c - W/2$. When present, the PSs quantization errors are $\delta_i^t \sim \mathcal{U}(-\pi/4, \pi/4)$ while the TDLs errors are $\Delta\tau_i^t \sim \mathcal{U}(0, d_{\text{ant}}/c)$. The standard deviation of the time synchronization error is set to $\sigma_\epsilon = 1$ ns.

When operating at mm-wave frequencies, the path arrival time distributions can be described by a Poisson process and the inter-arrival times by an exponential probability density function [39]. The paths arrival rate is set to 4 [1/ns] while the paths azimuth and elevation angle-of-arrival (AOA) are modeled as uniformly distributed between $(0, 2\pi]$ and $(0, \pi]$, respectively. Note that these values are also in line with those found in [40], [41] where a mm-wave measurements campaign using massive arrays for radar-based mapping purposes have been described.

Before analyzing the MIMO and beamforming localization performance, it is necessary to ensure that the comparison based on CRB can be considered fair in terms of SNR working regimes when operating with non-massive arrays. To this purpose, a threshold in terms of SNR is derived in order to

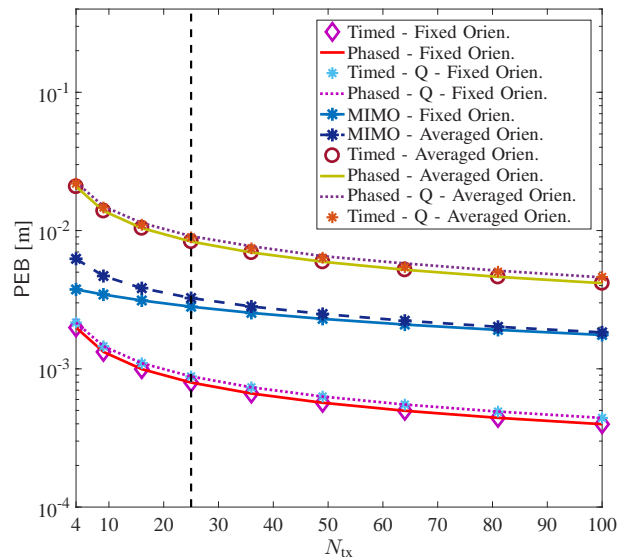


Fig. 4. PEB vs. N_{tx} , $N_{\text{rx}} = 25$ and orientation aware.

understand if ambiguities are significant or not and, hence, whether the CRB can still be used as a performance metric for comparison. In this perspective, we still consider the AF as a tool to investigate the performance of maximum likelihood estimator (MLE) as a function of the probability of ambiguity, i.e., secondary lobes higher than the main lobe. In fact, the AF main lobe determines the mean square error (MSE) behaviour in the high SNR region that is described by the CRB, while the AF sidelobes might generate ambiguities in case of large noise in the low SNR region and that are not taken into account by the CRB. The details of the aforementioned analysis are reported in Appendix D.

In our numerical results, for each tested configuration we verified that the SNR level is above a threshold calculated to guarantee that the probability of ambiguity is less than 10^{-2} .

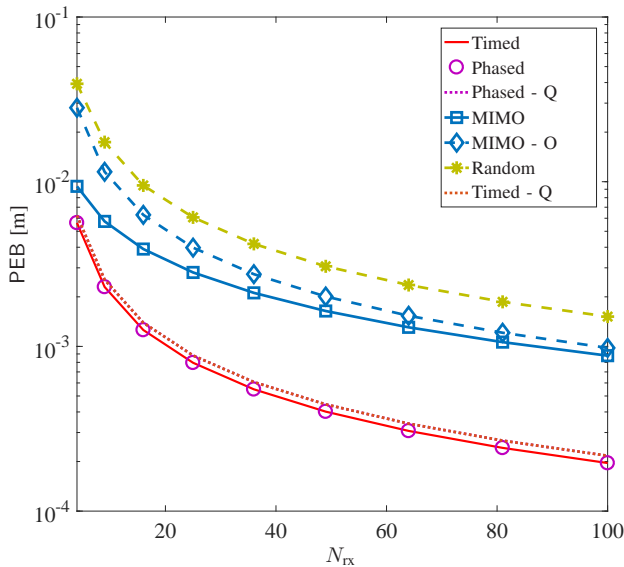
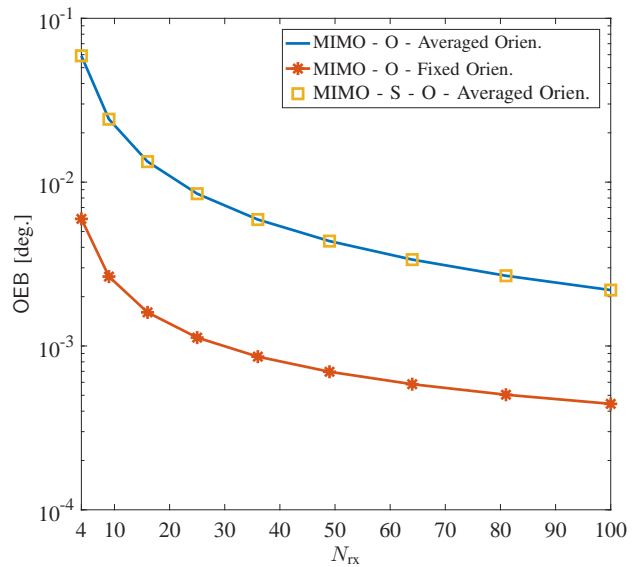
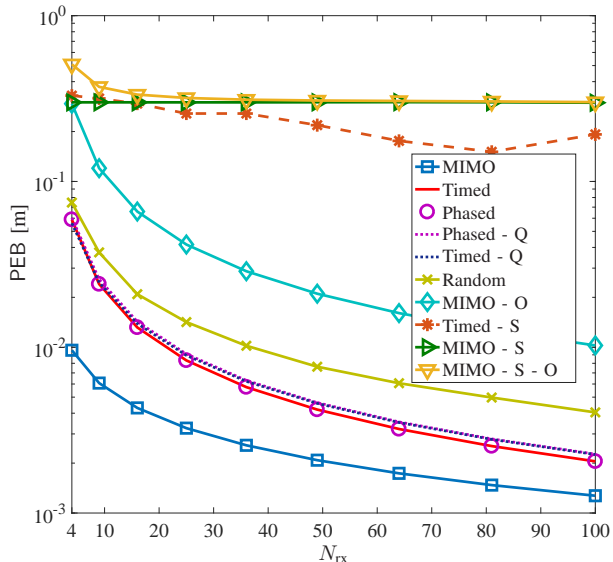
B. Results

The results of this section have been obtained as a function of N_{tx} and N_{rx} ; the array structure (i.e. timed, phased, random, MIMO); the presence and absence of array beamforming and of a residual time synchronization error; and the multipath overlapping effect.

1) Free space scenario:

a) *Results as a function of N_{tx}* : Figure 4 reports the PEB performance as a function of N_{tx} and of the Rx orientation in free-space. MIMO, timed and phased arrays (with and without quantization errors) are compared in the *orientation-aware* case when the number of receiving antennas is kept fixed to $N_{\text{rx}} = 25$.

It can be observed that MIMO arrays, relying on different transmitted waveforms, outperform timed and phased arrays in averaged orientations cases; whereas, in fixed Rx orientation, as described in Sec. VI, arrays operating beamforming exhibit a better performance. This is due to the fact that beamforming strategies (e.g., those adopted in timed and phased arrays) fail in preserving the same accuracy for any geometric configuration (i.e., for any Rx orientation). Contrarily, thanks to the


 Fig. 5. PEB vs. N_{rx} , $N_{tx} = 25$ and fixed receiver orientations.

 Fig. 7. OEB vs. N_{rx} , $N_{tx} = 25$.

 Fig. 6. PEB vs. N_{rx} , $N_{tx} = 25$ and averaged receiver orientation.

diversity gain characterizing MIMO arrays, Rx orientations have a less significant effect on positioning accuracy.

For what the beamforming arrays are concerned, it can be observed that, as expected, timed and phased arrays results coincide as $W/f_c \ll 1$. In fact, phased arrays are the best candidate to be adopted in narrowband systems where there is no need to compensate for delays to perform beamsteering operation. We refer the reader to our previous work [12] to better appreciate the impact of the fractional bandwidth on the timed/phased array performance.

Another important outcome from Fig. 4 is that array quantization errors, once characterized, slightly affect the localization performance. This implies that we can rely on simpler array structures (i.e., using switches instead of multipliers) without severely affecting the performance. Finally, with $N_{tx} \geq 25$, the performance improvement becomes less

important if a sufficiently high N_{tx} is considered. This implies that N_{tx} can be relaxed to shrink the array dimensions and to enable the integration on mobiles [9]. Consequently, in the following, the number of transmitting antennas will be fixed to $N_{tx} = 25$.

b) Results as a function of N_{rx} : In Fig. 5, the PEB performance are reported for both *orientation-aware* and *-unaware* cases as a function of N_{rx} in free-space propagation condition, $N_{tx} = 25$ and fixed Tx and Rx orientation $\vartheta^t = \vartheta^r = [0, 0]^T$. The results have been obtained using the analytic expressions (42), (44) and (45) and reveal that arrays performing beamforming outperform the performance of MIMO for the particular steering and geometric configuration conditions chosen, as already observed in Fig. 4. We ascribe the effect to an increased SNR in the considered direction. Nevertheless, with arrays operating single-beam beamforming, orientation estimation is not always possible and consequently the FIM results to be singular. Matrix singularity or ill-conditioning are, here, synonymous of the impossibility to estimate the position/orientation given the collected measurements.

Figure 6 shows the average PEB performance when the Rx orientation randomly changes at each Monte Carlo iteration. For this analysis, we consider also random weighting, quantization errors as well as time synchronization mismatch between the Tx and the Rx. The positioning performance are shown for the *orientation-aware* case if not otherwise indicated. As in Figs. 4-5, the performance of timed and phased arrays coincide due to the narrow fractional bandwidth (i.e., $W/f_c \approx 0.016$). Differently from Fig. 5, in Fig. 6 MIMO achieves a higher positioning accuracy with respect to arrays employing beamforming strategies due to the fact that results are averaged over different Rx orientations. In fact, with MIMO, a reduction in the received SNR is experienced, but the number of independent measurements is maximized (i.e., $N_{tx}N_{rx}$).

For what random weighting arrays are regarded, they share

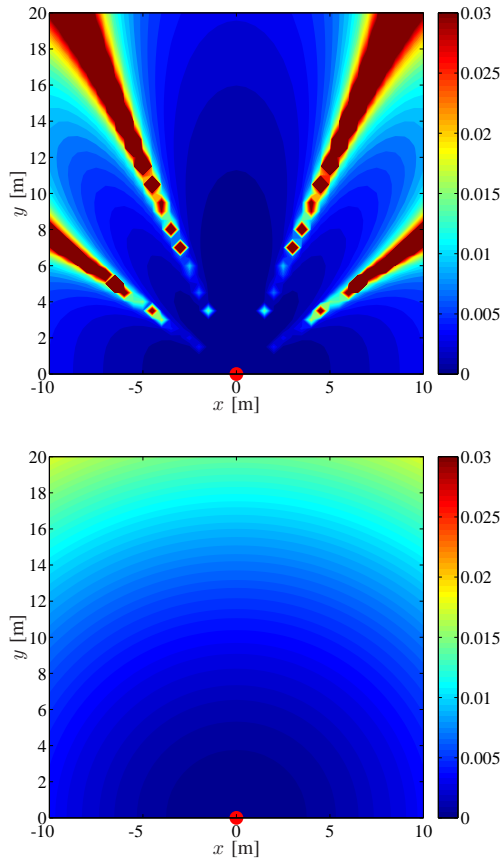


Fig. 8. Phased (top) and MIMO (bottom) array PEB, $N_{rx} = 100$, $N_{tx} = 25$ and averaged receiver orientations.

the structure simplicity of phased arrays but they neither perform beamforming nor achieve the diversity gain of MIMO, and thus, the positioning accuracy results degraded with respect to other structures. Nevertheless, if the localization accuracy required by the application of interest is not so stringent, they could be an interesting option to guarantee both a sub-centimeter positioning accuracy (e.g., for $N_{rx} = 50$ and $N_{tx} = 25$, $PEB \approx 7$ mm) and an easy implementation in future mobiles and AP operating at mm-wave frequencies.

Note that when the Tx orientation is one of the parameters to be estimated (*orientation-unaware* case), only MIMO results in a non-singular FIM. Obviously, in this case, given the reduced information available at the Rx side, the positioning accuracy worsen with respect to the *orientation-aware* case. In all cases, the residual time synchronization error degrades the localization performance.

Figure 7 reports the OEB as a function of N_{rx} . In this case, only the performance of MIMO is present because of the singularity problem arising in timed, phased and random weighting arrays. An interesting results is that, in this case, time synchronization error does not impact the orientation accuracy.

c) *Grid results*: Figure 8 reports the PEB results for the *orientation-aware* case when the mobile moves in a grid of points spaced of 0.5 m considering phased (Fig. 8-top) and MIMO (Fig. 8-bottom) arrays, respectively. We considered a

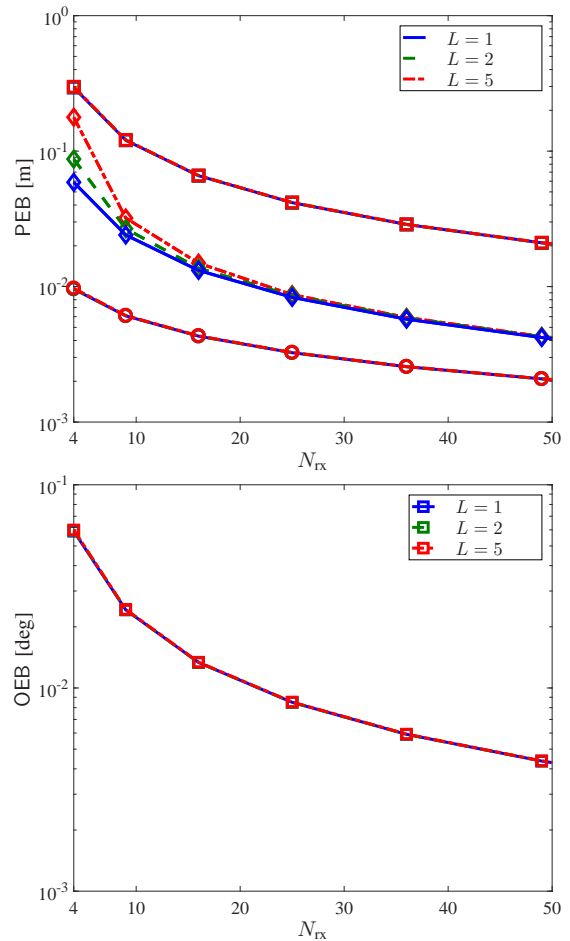


Fig. 9. PEB and OEB vs. N_{rx} in multipath propagation scenario, $N_{tx} = 25$, $W = 1$ GHz, averaged receiver orientation. Diamond marked lines refer to phased array, circle marked lines to MIMO, and square marked lines to MIMO orientation unaware.

3D indoor scenario of $10 \times 10 \times 3$ m³ where the mobile and the AP centroids are at the same height. The Rx, equipped with $N_{rx} = 100$ antennas, is placed in $\mathbf{p}^r = [0, 0, 0]^T$ with orientation changing at each Monte Carlo iteration. On the other side, the mobile array is equipped with $N_{tx} = 25$ and its orientation and its steering direction are fixed to $\vartheta^t = [0, 0]^T$ and to the broadside direction, respectively. Grid results confirm that MIMO arrays localization performance does not depend on the Rx orientation and on mobile position in space but only on the distance between the Tx and the Rx. Indeed, when comparing Fig. 8-top and Fig. 8-bottom, it can be seen that if the mobile steering is fixed, the localization accuracy is higher in a privileged direction in space corresponding to the best geometric configuration conditions.

2) Multipath scenario:

a) *Results as a function of N_{rx}* : Figure 9 investigates the multipath effect by analysing the PEB and OEB averaged over different Rx orientations and as a function of the number of MPCs for phased and MIMO arrays. We consider the statistical multipath parameters described in Sec. VIII-A. As foreseen in the asymptotic analysis in Sec. VII, when increasing N_{rx} , the MPCs effect becomes negligible and the performance tends to coincide with that obtained in free-space. Moreover, it is

possible to remark that phased arrays are more sensitive to multipath with respect to MIMO arrays, especially when the number of receiving antennas is small. In fact, for phased arrays at least $N_{\text{tx}} = 25$ and $N_{\text{rx}} = 25$ are necessary to make the MPCs fully resolvable. In any case, it is interesting to note that to make the impact of MPCs negligible the antenna arrays are not required to be significantly massive.

IX. CONCLUSION

In this paper, we have considered a new scenario where a single-anchor localization exploiting mm-wave massive arrays has been put forth for next 5G applications. The theoretical localization performance has been evaluated by deriving the position and orientation CRB for different array configurations. Phase quantization, the residual time synchronization mismatch, and multipath have been considered as nuisance parameters. The comparison between MIMO and beamforming has been carried out by analyzing the impact of the number of antenna elements on the performance. From analytical and simulation results, the main conclusions and achievements emerged in this paper can be summarized as follows:

- We show through an asymptotic analysis (i.e., $N_{\text{rx}} \rightarrow \infty$) that the considered CRB is a tight bound regardless the propagation condition and the array configuration considered.
- A beamforming with steering capability is desirable to maximize the SNR towards a specific direction, as happens for phased and timed arrays; but it reduces the diversity gain (typical of MIMO) exploitable for retrieving positioning information, especially in *orientation-unaware* situations.
- Quantization errors slightly impact the localization performance of both timed and phased arrays. Consequently, the array design requirements can be relaxed in favor of lower complexity and cost.
- Both for MIMO and beamforming, a time synchronization mismatch between the Tx and the Rx significantly degrades the positioning performance. From this point-of-view, it is important to minimize the clock mismatch between the arrays. Contrarily, in the *orientation-unaware* case, the time synchronization error does not affect the performance of the estimation;
- The adoption of multiple antennas makes the positioning insensitive to multipath for most of geometric configurations. This is true even when the number of antennas is not extremely high (i.e., $N_{\text{tx}}, N_{\text{rx}} > 20$); we demonstrated such point also through an asymptotic analysis.
- Finally, random weighting results to be a good low-complexity strategy to achieve centimeter level accuracy.

APPENDIX A

Considering the sub-set of random parameters $\boldsymbol{\psi}_r = [\boldsymbol{\kappa}_2^T, \dots, \boldsymbol{\kappa}_L^T, \epsilon^s]^T = [\boldsymbol{\alpha}^{\mathfrak{R}\tau}, \boldsymbol{\alpha}^{\mathfrak{S}\tau}, \epsilon^s]^T$, and treating them as independent RVs we can write

$$\ln(f(\boldsymbol{\psi}_r)) = \ln(f(\boldsymbol{\alpha}^{\mathfrak{R}\tau})) + \ln(f(\boldsymbol{\alpha}^{\mathfrak{S}\tau})) + \ln(f(\epsilon^s)). \quad (52)$$

Therefore, the elements of the *a-priori* FIM are

$$J_{\epsilon^s \epsilon^s}^p = \frac{1}{\sigma_\epsilon^2}, \quad J_{\alpha_k^{\mathfrak{R}} \alpha_l^{\mathfrak{R}}}^p = J_{\alpha_k^{\mathfrak{S}} \alpha_l^{\mathfrak{S}}}^p = \begin{cases} \frac{1}{\sigma_l^2} & \text{if } l = k \\ 0 & \text{if } l \neq k \end{cases}. \quad (53)$$

APPENDIX B

In this Appendix we derive the elements of the data FIM reported in (19). To accomplish this task, we introduce the following quantities

$$\begin{aligned} \chi_{ij}^{(l,k)}(p) &= \int_W \tilde{b}_{ij}(f) (f + f_c)^p e^{-j2\pi f \Delta\tau_{ij}^{(l,k)}} P_i(f) P_j^*(f) df \\ R_{ij}^p(\Delta\tau) &= \int_W \tilde{b}_{ij}(f) e^{-j2\pi f \Delta\tau} P_i(f) P_j^*(f) df \\ R_{ij}^{\ddot{p}}(\Delta\tau) &= \int_W \tilde{b}_{ij}(f) f^2 e^{-j2\pi f \Delta\tau} P_i(f) P_j^*(f) df \end{aligned} \quad (57)$$

where $\Delta\tau_{ij}^{(l,k)} = \tau_{iml} - \tau_{jmk}$, $\tilde{b}_{ij}(f) = \tilde{b}_i(f) \tilde{b}_j^*(f)$, and $\tilde{b}_i^c = \tilde{b}_i^c \left(\tilde{b}_i^c\right)^*$. The elements of $\mathbf{J}_{\mathbf{q}\mathbf{q}}^d$ can be expressed as in (33).

The elements of $\mathbf{J}_{\boldsymbol{\kappa}\boldsymbol{\kappa}}^d$ are

$$\begin{aligned} J_{a_1 a_1} &= 2\nu \sum_{mij} \Re \left\{ \tilde{b}_{ij}^c \xi_{ij}^{(1,1)} R_{ij}^p \left(\Delta\tau_{ij}^{(1,1)} \right) \right\} \\ J_{\alpha_k^{\mathfrak{R}} \alpha_1} &= J_{\alpha_1 \alpha_k}^{\mathfrak{H}} = 2\nu \sum_{mij} \Re \left\{ \tilde{b}_{ij}^c \xi_{ij}^{(1,k)} R_{ij}^p \left(\Delta\tau_{ij}^{(1,k)} \right) \right\} \\ J_{\alpha_k^{\mathfrak{S}} \alpha_1} &= J_{\alpha_1 \alpha_k}^{\mathfrak{H}} = 2\nu \sum_{mij} \Im \left\{ \tilde{b}_{ij}^c \xi_{ij}^{(1,k)} R_{ij}^p \left(\Delta\tau_{ij}^{(1,k)} \right) \right\} \\ J_{\alpha_k^{\mathfrak{R}} \alpha_l^{\mathfrak{R}}} &= J_{\alpha_k^{\mathfrak{S}} \alpha_l^{\mathfrak{S}}} = 2\nu \sum_{mij} \Re \left\{ \tilde{b}_{ij}^c \xi_{ij}^{(l,k)} R_{ij}^p \left(\Delta\tau_{ij}^{(l,k)} \right) \right\} \\ J_{\alpha_k^{\mathfrak{S}} \alpha_l^{\mathfrak{R}}} &= J_{\alpha_l^{\mathfrak{R}} \alpha_k^{\mathfrak{S}}} = 2\nu \sum_{mij} \Im \left\{ \tilde{b}_{ij}^c \xi_{ij}^{(l,k)} R_{ij}^p \left(\Delta\tau_{ij}^{(l,k)} \right) \right\} \end{aligned}$$

where $\xi_{ij}^{(l,k)} = e^{-j2\pi f_c(\tau_{im1} + \epsilon^s + \tau_m^r(\boldsymbol{\theta}_k) - \tau_j^l(\boldsymbol{\theta}_k))}$ and $\xi_{ij}^{(l,k)} = e^{-j2\pi f_c(-\tau_m^r(\boldsymbol{\theta}_l) + \tau_m^r(\boldsymbol{\theta}_k) + \tau_i^l(\boldsymbol{\theta}_l) - \tau_j^l(\boldsymbol{\theta}_k))}$.

The elements of $\mathbf{J}_{\mathbf{q}\boldsymbol{\kappa}}^d$ are

$$\begin{aligned} J_{q a_1} &= 4\pi a_1 \nu \sum_{mij} \Im \left\{ \tilde{b}_{ij}^c \xi_{ij}^{(1,1)} \chi_{ij}^{(1,1)}(1) \right\} \nabla_q (\tau_{im1}) = 0 \\ J_{q \alpha_k^{\mathfrak{R}}} &= -4\pi a_1 \nu \sum_{mij} \Im \left\{ \tilde{b}_{ij}^c \xi_{ij}^{(k,1)} \chi_{ij}^{(k,1)}(1) \right\} \nabla_q (\tau_{jm1}) \\ J_{q \alpha_k^{\mathfrak{S}}} &= 4\pi a_1 \nu \sum_{mij} \Re \left\{ \tilde{b}_{ij}^c \xi_{ij}^{(k,1)} \chi_{ij}^{(k,1)}(1) \right\} \nabla_q (\tau_{im1}) \end{aligned} \quad (58)$$

where $\xi_{ij}^{(k,1)} = e^{-j2\pi f_c(-\tau_{jm1} - \epsilon^s - \tau_m^r(\boldsymbol{\theta}_k) + \tau_i^l(\boldsymbol{\theta}_k))}$. Note that $\mathbf{J}_{\boldsymbol{\kappa}\boldsymbol{\kappa}}^d = \mathbf{J}_{\mathbf{q}\boldsymbol{\kappa}}^{\mathfrak{dH}}$.

Now, if we consider the presence of a residual time synchronization error, the FIM $\mathbf{J}_{\epsilon^s \epsilon^s}^d$ is

$$\begin{aligned} J_{\epsilon^s \epsilon^s} &= 8\pi^2 \nu \Re \left\{ \sum_{mij} \tilde{b}_{ij}^c \left[a_1^2 \xi_{ij}^{(1,1)} \chi_{ij}^{(1,1)}(2) + \right. \right. \\ &\quad \left. \left. + \sum_{k=2}^L \sigma_l^2 R_{ij}^{\ddot{p}} \left(\Delta\tau_{ij}^{(k,k)} \right) e^{-j2\pi f_c(\tau_i^l(\boldsymbol{\theta}_k) - \tau_j^l(\boldsymbol{\theta}_k))} \right] \right\}. \end{aligned}$$

$$\nabla_{\mathbf{q}\mathbf{q}}(\tau_{im1}, \tau_{jm1}) = \frac{d_{\text{ant}}^2}{(cy)^2} \begin{bmatrix} (m_x - i_x)(m_x - j_x) & \frac{y}{d_{\text{ant}}} (m_x - i_x) & (m_x - i_x)(j_z - m_z) & y(i_x - m_x)j_z \dots & y(i_x - m_x)j_x \\ \dots & \frac{y}{d_{\text{ant}}} & \frac{y}{d_{\text{ant}}}(j_z - m_z) & -\frac{y^2}{d_{\text{ant}}}j_z & -\frac{y^2}{d_{\text{ant}}}j_x \\ \dots & \dots & (i_z - m_z)(j_z - m_z) & y(m_z - i_z)j_z & y(m_z - i_z)j_x \\ \dots & \dots & \dots & y^2i_zj_z & y^2i_zj_x \\ \dots & \dots & \dots & \dots & y^2i_xj_x \end{bmatrix} \quad (54)$$

$$\text{CRB}(\mathbf{q}) = \frac{c^2}{8\pi^2 N_{\text{tx}} \text{SNR}_1 (\beta_i^2 + f_c^2)} \frac{1}{S} \begin{bmatrix} \frac{12}{(N_{\text{rx}}-1)} & 0 & 0 & 0 & \frac{12}{y(1-N_{\text{rx}})} \\ 0 & \frac{S}{N_{\text{rx}}} & 0 & 0 & 0 \\ 0 & 0 & \frac{12}{(N_{\text{rx}}-1)} & \frac{12}{y(1-N_{\text{rx}})} & 0 \\ 0 & 0 & \frac{12}{y(1-N_{\text{rx}})} & \frac{12(N_{\text{rx}}+N_{\text{rx}}-2)}{y^2(N_{\text{rx}}-1)(N_{\text{rx}}-1)} & 0 \\ \frac{12}{y(1-N_{\text{rx}})} & 0 & 0 & 0 & \frac{12(N_{\text{rx}}+N_{\text{rx}}-2)}{y^2(N_{\text{rx}}-1)(N_{\text{rx}}-1)} \end{bmatrix} \quad (55)$$

$$\text{CRB}(\mathbf{p}^1) = \frac{c^2}{8\pi^2 N_{\text{tx}} \text{SNR}_1 (\beta^2 + f_c^2)} \frac{1}{S} \text{diag} \left(\frac{12}{N_{\text{tx}}(N_{\text{rx}}-1)}, \frac{S}{N_{\text{tx}} N_{\text{rx}}}, \frac{12}{N_{\text{tx}}(N_{\text{rx}}-1)} \right) \quad (56)$$

The elements of $\mathbf{J}_{\kappa\epsilon^s}^{\text{d}}$ are

$$J_{a_1 \epsilon^s} = 4\pi a_1 \nu \sum_{mij} \Im \left\{ \tilde{b}_{ij}^c \xi_{ij}^{(1,1)} \chi_{ij}^{(1,1)}(1) \right\}$$

$$J_{\alpha_k^{\Re} \epsilon^s} = 4\pi a_1 \nu \sum_{mij} \Im \left\{ \tilde{b}_{ij}^c \xi_{ij}^{(1,k)} \chi_{ij}^{(1,k)}(1) \right\}$$

$$J_{\alpha_k^{\Im} \epsilon^s} = 4\pi a_1 \nu \sum_{mij} \Re \left\{ \tilde{b}_{ij}^c \xi_{ij}^{(1,k)} \chi_{ij}^{(1,k)}(1) \right\}.$$

As before the elements of $\mathbf{J}_{\epsilon^s \kappa}^{\text{d}}$ could be found as $\mathbf{J}_{\epsilon^s \kappa}^{\text{d}} = \mathbf{J}_{\kappa\epsilon^s}^{\text{dH}}$. Finally, the elements of $\mathbf{J}_{\mathbf{q}\epsilon^s}^{\text{d}}$ are

$$J_{q\epsilon^s} = 8\pi^2 \nu a_1^2 \sum_{mij} \Re \left\{ \tilde{b}_{ij}^c \xi_{ij}^{(1,1)} \chi_{ij}^{(1,1)}(2) \right\} \nabla_{\mathbf{q}}(\tau_{jm1})$$

and $\mathbf{J}_{\epsilon^s \mathbf{q}}^{\text{d}} = \mathbf{J}_{\mathbf{q}\epsilon^s}^{\text{dH}}$.

APPENDIX C

In this Appendix we will specialize the expression of the symmetric matrix \mathbf{G} reported in (38)-(39). To this end, we explicit the geometric relationship relating the TOA between each TX-RX antennas couple and the considered localization (position or orientation) parameter, i.e., $\nabla_{q_a q_b}(\tau_{iml}, \tau_{jml}) = \nabla_{q_a}(\tau_{iml}) \nabla_{q_b}(\tau_{jml})$. For the particular antenna configuration chosen described in Sec. II-B, in which the array antennas are spaced of d_{ant} , and considering $\vartheta^t = [0, 0]^T$, we can compute a simplified version of (35)-(37). Specifically, it is possible to obtain:

$$\nabla_p(\tau_{im1}) = \frac{1}{c} [c \nabla_p(\tau_1) + d_{\text{ant}} ((i_x - m_x) \nabla_p(\phi_1) + (m_z - i_z) \nabla_p(\theta_1))] \quad (59)$$

$$\nabla_{\vartheta^t}(\tau_{im1}) = -\frac{d_{\text{ant}}}{c} i_z, \quad \nabla_{\varphi^t}(\tau_{im1}) = -\frac{d_{\text{ant}}}{c} i_x \quad (60)$$

with $m_x = m_z = -\frac{\sqrt{N_{\text{rx}}-1}}{2}, -\frac{\sqrt{N_{\text{rx}}-1}}{2} + 1, \dots, \frac{\sqrt{N_{\text{rx}}-1}}{2}$ and $i_x = i_z = j_x = j_z = -\frac{\sqrt{N_{\text{tx}}-1}}{2}, -\frac{\sqrt{N_{\text{tx}}-1}}{2} + 1, \dots, \frac{\sqrt{N_{\text{tx}}-1}}{2}$. From (59)-(60), it is straightforward to derive (54). Then, by considering the summations present in \mathbf{G} , it is possible to obtain the CRB matrices for MIMO and timed arrays respectively as in (55)-(56) where $S = A^t/y^2$.

TABLE II
MIMO VS. BEAMFORMING COMPARISON

MIMO/Timed	N_{rx}	γ [dB]	σ_{thr} [mV]	σ_{sim} [mV]
MIMO	4	-36.9	0.062	0.022
MIMO	36	-32.1	0.187	0.022
MIMO	100	-29.9	0.313	0.022
Phased	4	-33.5	0.136	0.022
Phased	36	-28.7	0.406	0.022
Phased	100	-26.5	0.677	0.022

APPENDIX D

In this Appendix we consider the AF as defined in (22).

The AF for the position coordinates shows a main peak in correspondence of the true Tx position and secondary sidelobes peaks relative to ‘‘wrong’’ positions. An ambiguity problem arises when one of these sidelobes overcomes or becomes comparable to the main beam due to noise. Consequently, to determine whether ambiguities are negligible in the non-massive array case, we have derived a threshold on the noise standard deviation in order to keep the ambiguity probability fixed to a desired low value.

By comparing the threshold obtained with the value used in the numerical results, we can demonstrate that we operate at a high SNR regime where the CRB is tight even if a non-massive array is adopted.

To this end, we define the ambiguity probability as [35]

$$P_A = \frac{1}{2} \text{erfc} \left(\frac{\gamma}{\sqrt{4\sigma^2}} \right) \quad (61)$$

where σ is the noise standard deviation and γ is the gap between the main lobe of the AF and the highest secondary

sidelobe. Then, given a certain gap γ , it is possible to compute the noise threshold as

$$\sigma_{\text{thr}} = \frac{\gamma}{2} \frac{1}{\text{erfc}^{-1}(2P_A^*)}. \quad (62)$$

In Table II, we report the obtained simulation results. We have considered the Tx moving in a grid of points spaced apart of 0.2 m in a cube of dimension $8 \times 8 \times 8 \text{ m}^3$. The target ambiguity probability has been fixed to 10^{-2} . The gap γ has been set to the minimum side-lobe level considering the three spatial coordinates (that is, to the worst case scenario). σ_{sim} represents the noise standard deviation used in the numerical results of the paper.

As one can notice, in all the tested configurations the noise standard deviation used in the numerical results is always much lower than the threshold σ_{thr} above that the ambiguity effect is not anymore negligible.

The proposed method is a useful tool to test whether a specific scenario can be considered in the asymptotic regime and, hence, the CRB can be a meaningful metric.

REFERENCES

- [1] W. H. Chin, Z. Fan, and R. Haines, "Emerging technologies and research challenges for 5G wireless networks," *IEEE Wireless Commun.*, vol. 21, no. 2, pp. 106–112, 2014.
- [2] V. Khaitan, P. Tinnakornsrisuphap, and M. Yavuz, "Indoor positioning using femtocells," in *Proc. IEEE Veh. Technol. Conf. (VTC Fall)*, 2011, pp. 1–5.
- [3] E. G. Larsson *et al.*, "Massive mimo for next generation wireless systems," *IEEE Commun. Mag.*, vol. 52, no. 2, pp. 186–195, 2014.
- [4] F. Rusek *et al.*, "Scaling up MIMO: Opportunities and challenges with very large arrays," *IEEE Signal Process. Mag.*, vol. 30, no. 1, pp. 40–60, 2013.
- [5] A. L. Swindlehurst *et al.*, "Millimeter-wave massive MIMO: The next wireless revolution?" *IEEE Commun. Mag.*, vol. 52, no. 9, pp. 56–62, 2014.
- [6] R. Di Taranto *et al.*, "Location-aware communications for 5G networks: How location information can improve scalability, latency, and robustness of 5G," *IEEE Signal Process. Mag.*, vol. 31, no. 6, pp. 102–112, 2014.
- [7] F. Guidi, A. Guerra, and D. Dardari, "Personal mobile radars with millimeter-wave massive arrays for indoor mapping," *IEEE Trans. Mobile Comput.*, vol. 15, no. 6, pp. 1471–1484, 2016.
- [8] D. Dardari, P. Closas, and P. M. Djurić, "Indoor tracking: Theory, methods, and technologies," *IEEE Trans. Veh. Technol.*, vol. 64, no. 4, pp. 1263–1278, 2015.
- [9] W. Hong *et al.*, "Study and prototyping of practically large-scale mmwave antenna systems for 5G cellular devices," *IEEE Commun. Mag.*, vol. 52, no. 9, pp. 63–69, 2014.
- [10] S. M. Razavizadeh, M. Ahn, and I. Lee, "Three-dimensional beamforming: A new enabling technology for 5G wireless networks," *IEEE Signal Process. Mag.*, vol. 31, no. 6, pp. 94–101, 2014.
- [11] K. Witrisal *et al.*, "High-accuracy localization for assisted living: 5G systems will turn multipath channels from foe to friend," *IEEE Signal Process. Mag.*, vol. 33, no. 2, pp. 59–70, 2016.
- [12] A. Guerra, F. Guidi, and D. Dardari, "Position and orientation error bound for wideband massive antenna arrays," in *Proc. IEEE Int. Conf. on Commun. Workshop (ICCW)*, 2015, pp. 853–858.
- [13] N. Garcia *et al.*, "Direct localization for massive MIMO," *arXiv preprint arXiv:1607.00946*, 2016.
- [14] H. Kaouach *et al.*, "Wideband low-loss linear and circular polarization transmit-arrays in V-band," *IEEE Trans. Antennas Propag.*, vol. 59, no. 7, pp. 2513–2523, 2011.
- [15] A. Clemente *et al.*, "Wideband 400-element electronically reconfigurable transmitarray in X band," *IEEE Trans. Antennas Propag.*, vol. 61, no. 10, pp. 5017–5027, 2013.
- [16] F. Guidi *et al.*, "Joint energy detection and massive array design for localization and mapping," *IEEE Trans. Wireless Commun.*, vol. 16, no. 3, pp. 1359–1371, March 2017.
- [17] Y. Shen and M. Z. Win, "On the accuracy of localization systems using wideband antenna arrays," *IEEE Trans. Commun.*, vol. 58, no. 1, pp. 270–280, 2010.
- [18] —, "Fundamental limits of wideband localization part I: A general framework," *IEEE Trans. Inf. Theory*, vol. 56, no. 10, pp. 4956–4980, 2010.
- [19] Y. Han *et al.*, "Performance limits and geometric properties of array localization," *IEEE Trans. Inf. Theory*, vol. 62, no. 2, pp. 1054–1075, 2016.
- [20] A. Shahmansoori *et al.*, "5G position and orientation estimation through millimeter wave MIMO," in *Proc. IEEE Global Conf. on Commun. (GLOBECOM) Workshops*, 2015, pp. 1–6.
- [21] A. Mallat and L. Vandendorpe, "CRBs for the joint estimation of TOA and AOA in wideband MISO and MIMO systems: comparison with SISO and SIMO systems," in *Proc. IEEE Int. Conf. on Commun.*, 2009, pp. 1–6.
- [22] A. Guerra, F. Guidi, and D. Dardari, "On the Impact of Beamforming Strategy on mm-Wave Localization Performance Limits," in *Proc. IEEE Int. Conf. on Commun. Workshop (ICCW)*.
- [23] T. M. Cover and J. A. Thomas, *Elements of information theory*. John Wiley & Sons, 2012.
- [24] A. Alkhateeb *et al.*, "Channel estimation and hybrid precoding for millimeter wave cellular systems," *IEEE J. Sel. Topics Signal Process.*, vol. 8, no. 5, pp. 831–846, 2014.
- [25] N. Garcia *et al.*, "Location-aided mm-wave channel estimation for vehicular communication," in *2016 IEEE 17th Int. Workshop on Signal Process. Advances in Wireless Commun. (SPAWC)*. IEEE, 2016, pp. 1–5.
- [26] D. Dardari *et al.*, "Ranging with ultrawide bandwidth signals in multipath environments," *Proc. IEEE*, vol. 97, no. 2, pp. 404–426, 2009.
- [27] J. Li and P. Stoica, "MIMO radar with colocated antennas," *IEEE Signal Process. Mag.*, vol. 24, no. 5, pp. 106–114, 2007.
- [28] E. Fishler *et al.*, "Spatial diversity in radars-models and detection performance," *IEEE Trans. Signal Process.*, vol. 54, no. 3, pp. 823–838, 2006.
- [29] A. Hassanien and S. A. Vorobyov, "Phased-MIMO radar: A tradeoff between phased-array and MIMO radars," *IEEE Trans. Signal Process.*, vol. 58, no. 6, pp. 3137–3151, 2010.
- [30] Q. He *et al.*, "Target velocity estimation and antenna placement for MIMO radar with widely separated antennas," *IEEE J. Sel. Topics Signal Process.*, vol. 4, no. 1, pp. 79–100, 2010.
- [31] A. M. Haimovich, R. S. Blum, and L. J. Cimini, "MIMO radar with widely separated antennas," *IEEE Signal Process. Mag.*, vol. 25, no. 1, pp. 116–129, 2008.
- [32] A. F. Molisch, *Wireless communications*. John Wiley & Sons, 2007.
- [33] H. Godrich, A. M. Haimovich, and H. V. Poor, "An analysis of phase synchronization mismatch sensitivity for coherent MIMO radar systems," in *Proc. 3rd IEEE Int. Workshop Comput. Adv. in Multi-Sensor Adaptive Process. (CAMSAP)*, 2009, pp. 153–156.
- [34] K. Witrisal and P. Meissner, "Performance bounds for multipath-assisted indoor navigation and tracking (MINT)," in *Proc. IEEE Int. Conf. Commun. (ICC)*, 2012, pp. 4321–4325.
- [35] H. L. Van Trees, *Detection, estimation, and modulation theory*. John Wiley & Sons, 2004.
- [36] G. San Antonio, D. R. Fuhrmann, and F. C. Robey, "MIMO radar ambiguity functions," *IEEE J. Sel. Topics in Signal Process.*, vol. 1, no. 1, pp. 167–177, 2007.
- [37] A. W. Van der Vaart, *Asymptotic statistics*. Cambridge university press, 2000, vol. 3.
- [38] FCC, "Revision of Part 15 of the Commissions Rules Regarding Operation in the 57-64 GHz Band. August 2013."
- [39] C. Gustafson *et al.*, "On mm-wave multipath clustering and channel modeling," *IEEE Trans. Antennas Propag.*, vol. 62, no. 3, pp. 1445–1455, 2014.
- [40] A. Guerra *et al.*, "Delay spread characterization of millimeter-wave indoor backscattering channel," in *Proc. 10th European Conf. Antennas and Propag. (EuCAP)*, 2016, pp. 1–2.
- [41] F. Guidi, A. Clemente, and R. D'Errico, "Multipath estimation technique for wideband mm-wave backscattering channels," in *Proc. 11th European Conf. Antennas and Propag. (EuCAP)*. IEEE, 2017.